J. Fluid Mech. (2005), *vol.* 543, *pp.* 203–237. © 2005 Cambridge University Press
doi:10.1017/S0022112005006361 Printed in the United Kingdom

A reduced-order partial differential equation model for the flow in a thermosyphon

By E. A. BURROUGHS[1], E. A. COUTSIAS[2] AND L. A. ROMERO[3]

[1]Department of Mathematics, Humboldt State University, Arcata, CA 95521, USA
burroughs@humboldt.edu

[2]Department of Mathematics and Statistics, University of New Mexico, Albuquerque, NM 87131, USA
vageli@math.unm.edu

[3]Department of Computational Mathematics and Algorithms,
Sandia National Laboratories, Albuquerque, NM 87185-1110, USA
lromero@sandia.gov

(Received 11 November 2004 and in revised form 17 May 2005)

Flow in a closed-loop thermosyphon heated from below exhibits a sequence of bifurcations with increasing Grashof number. Using the Navier–Stokes equations in the Boussinesq approximation we have derived a model where, in the case of a slender circular loop, the first Fourier modes exactly decouple from all other Fourier modes, leaving a system of three coupled nonlinear partial differential equations that completely describes the flow in the thermosyphon. We have characterized the flow through two bifurcations, identifying stable periodic solutions for flows of Prandtl number greater than 18.5, a much lower value than predicted previously. Because of the quadratic nonlinearity in this system of equations, it is possible to find the global stability limit, and we have proved that it is identical to the first bifurcation point.

The numerical study of the model equations is based on a highly accurate Fourier–Chebyshev spectral method, combined with asymptotic analysis at the various bifurcation points. Three-dimensional computations with a finite element method computational fluid dynamics code (MPSalsa), are also pursued. All three approaches are in close agreement.

1. Introduction

When a closed vertical loop of fluid is heated from below, a sequence of bifurcations ensues, leading from pure conduction to a convective unidirectional flow and then to periodic or chaotic flow. This is the problem of convection in a closed-loop thermosyphon, also called a natural convection loop. This problem has implications for the performance of heating/cooling systems (Martin & Sloley 1995; Japikse 1973). Moreover, it offers useful insights into general convective phenomena. The problem is appealing because of the possibility of observing complicated behaviour in a physically simple system.

Pioneering work in this field was done by Keller (1966) and Welander (1967) who identified that unsteady flow results directly from the dynamics of the system, rather than from an unsteady force. Recent mathematical models by Velázquez (1994) and Rodríguez-Bernal & Vleck (1998*b*) focus on the transition to complex dynamics. These works have modelled viscous and inertial terms with friction factors, leading to predictions of complex dynamical behaviour in qualitative agreement with observations. Also, recent works by Yuen & Bau (1996), Wang, Singer & Bau (1992), and Boskovic &

https://doi.org/10.1017/S0022112005006361 Published online by Cambridge University Press

Krstic (2001) have used feedback to control the onset of chaos. For a thorough survey of the early literature on this problem, see the review article by Greif (1988).

This problem is a variation of the well-studied Rayleigh–Bénard problem. In Rayleigh–Bénard convection, a layer of viscous fluid is heated from below. One finds that instability arises after a critical temperature gradient has been reached, and that the motions seen following this instability have a stationary cellular structure (Chandrasekhar 1961). Under suitable boundary conditions, a secondary structure arises where the fluid forms rolls, which undergo a Hopf bifurcation and become oscillatory (Salinger *et al.* 2005; Busse & Clever 1979; Willis & Deardorff 1970).

The Lorenz system, involving three ordinary differential equations, has most frequently been used as a model for the flow in a thermosyphon (Rodríguez-Bernal & Vleck 1998*a*; Greif 1988). In particular, the model displays periodic and chaotic flows for various parameter ranges (Lorenz 1963; Shimizu & Morioka 1978; Morioka & Shimizu 1978). Experimental studies also report oscillations for various parameter ranges (Stern, Greif & Humphrey 1988; Sano 1991). The Lorenz equations involve several parameters that must be measured experimentally or computed by making assumptions on the shapes of the temperature and velocity profiles in the thermosyphon. In this paper, rather than reducing the equations to a system of ordinary differential equations, we create a reduced-order set of partial differential equations involving only two spatial coordinates.

We derive this system of partial differential equations by assuming purely azimuthal (toroidal) flow along the loop. We represent the toroidal coordinate as a periodic axial direction, thus neglecting curvature effects along the loop, and we account for gravity effects through a gravity function that depends on the axial position. We are led in this way to a three-dimensional system of partial differential equations that makes the assumption that the flow at any cross-section is purely axial. For loops with small enough aspect ratio (the ratio of the radius of the cross-section to the length of the loop) we believe this assumption is well-justified. By using a modal expansion, these equations can be written as an infinite system of partial differential equations involving only two spatial coordinates. We show that for the case of a circular loop, this system rigorously reduces to a system of three partial differential equations, where the axial coordinate has been averaged out. We also show that for arbitrarily shaped symmetric loops, the linear stability of the conducting solution can be reduced to this same set of partial differential equations.

Our reduced-order system of partial differential equations has the advantage over the Lorenz model that no assumptions are needed about the shape of the velocity and temperature profiles. At the first bifurcation point, these profiles are found to be given by the Bessel function J_0 on the interval from zero to its first zero, γ_{01}. Although this function looks similar to a quadratic function, the result obtained from deriving the Lorenz equations based on the assumption that the profiles are quadratic is off by almost a factor of two in predicting the onset of convection. As the governing parameter, the Grashof number, is raised beyond its critical value, the profiles look increasingly less like quadratics. At Grashof numbers near the Hopf bifurcation point, there is little justification for assuming that the profiles are quadratic.

For the case of loops of circular cross-section, we assume solutions with radial symmetry, and our equations involve only one spatial coordinate. We use highly accurate spectral numerical methods to analyse this system. Excellent agreement is found between asymptotic analysis and simulations of the reduced model. Further comparisons of the predictions of the reduced model were pursued with numerical simulations of the full three-dimensional Navier–Stokes equations in the Boussinesq

https://doi.org/10.1017/S0022112005006361 Published online by Cambridge University Press

approximation, using the code MPSalsa (Salinger *et al.* 1999, 1996; Shadid *et al.* 1999), developed at Sandia National Laboratories to compute solutions to reacting flow problems on massively parallel computers. Again, good agreement was found in the ranges where the latter are feasible, i.e. around the onset of convection. However, full three-dimensional calculations near the Hopf bifurcation require prohibitively high resolution and they proved unfeasible.

Two dimensionless parameters characterize the flow: the Prandtl number Pr (2.13), a property of the fluid, the ratio of kinematic viscosity ν to thermal diffusivity κ, and the Grashof number Gr (2.14), which is proportional to the thermal gradient. Linearizing about the numerically computed purely conducting trivial state, one arrives at an eigenvalue problem from which we identify the onset of convection as a pitchfork bifurcation at a critical value of the Grashof number, Gr_p. This value is independent of the Prandtl number. Using energy methods, we formulate a variational problem that proves that the trivial solution is globally stable for $Gr < Gr_p$. We use continuation in Grashof number to numerically follow the convecting branch and also linearize the flow about the numerically computed convective state to determine the onset of a Hopf bifurcation at a second critical value, $Gr_h > Gr_p$. The oscillations found in the present model correspond to a pulsating flow where the period of oscillation is roughly equal to the time it takes for fluid to circulate around the loop.

The location of this Hopf bifurcation and its character are shown to be dependent on Pr. By numerically estimating the coefficients of a Landau equation describing the weakly nonlinear evolution of perturbations about the convective state near the Hopf bifurcation point, we show that the character of the bifurcation changes from subcritical to supercritical as Pr becomes larger than 18.5. For comparison we mention that the Prandtl numbers for water, alcohol, silicon oil, and glycerine, respectively, are 6.75, 16.6, 41, and 7250 (Landau & Lifshitz 1987).

We emphasize that the contributions this model makes to the study of the thermosyphon problem are that it captures the transition from the trivial to convective state in close agreement with full three-dimensional simulations, and it captures stable periodic flow. By assuming the flow profiles are radially symmetric, we allow for more complex profiles, as seen by experiments, than do Lorenz-type ordinary differential equation (ODE) models. Our model is limited in that it cannot capture asymmetric flow reversals, which become evident in experiments as the aspect ratio is increased. The model is valid for laminar flow in the range of Prandtl and Grashof numbers used in this work.

The outline for this paper is as follows. In § 2, we give a derivation of our partial differential equation (PDE) model and compare it to the common thermosyphon model, a Lorenz-like ODE model. Section 3 explores the stability of the trivial branch up to the first bifurcation point, a pitchfork bifurcation, and discusses its global stability. We also provide results of numerical calculations in two and three dimensions that validate our asymptotic analysis. In § 4 we analyse the stability of the convective branch, identify the second bifurcation as a Hopf bifurcation, and identify and analyse the transition between the regions of sub- and supercriticality of this bifurcation. In § 5 we present the numerical framework that we use in this research. Our conclusions are found in § 6.

2. Problem formulation

We study flow in a closed-loop thermosyphon – a tube which is bent into a vertical closed loop, heated symmetrically from below. The cross-section of the tube and the

https://doi.org/10.1017/S0022112005006361 Published online by Cambridge University Press

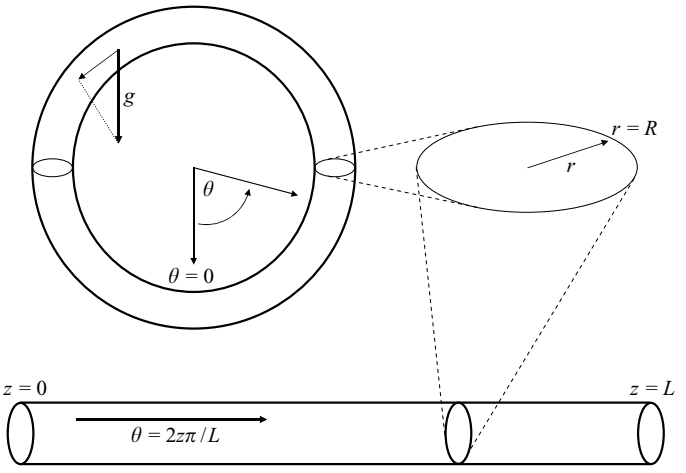


FIGURE 1. Problem geometry.

shape of the loop can be arbitrary, though the majority of this paper assumes a circular cross-section and circular loop.

We assume that the radius of the tube is small compared to its length, so that we can think of the flow as if it takes place in a straight tube with gravity a function of the axial distance along the tube. To achieve this reduction, periodic boundary conditions are imposed on all the model variables (see figure 1).

Begin with the Boussinesq equations

$$\nabla \cdot \boldsymbol{u} = 0, \tag{2.1}$$

$$\frac{\partial \boldsymbol{u}}{\partial t} + \boldsymbol{u} \cdot \nabla \boldsymbol{u} + \nabla \left(\frac{p}{\rho} \right) = \nu \nabla^2 \boldsymbol{u} + g\alpha (T - T_0) \boldsymbol{e}_z, \tag{2.2}$$

$$\frac{\partial T}{\partial t} + \boldsymbol{u} \cdot \nabla T = \kappa \nabla^2 T, \tag{2.3}$$

where $\boldsymbol{u}$ is velocity, p is pressure, T is temperature, and t is time, and the parameters are ρ (density), ν (kinematic viscosity), g (gravity), α (thermal expansion), and κ (thermal diffusivity). T_0 is a reference temperature, and $\boldsymbol{e}_z$ is the unit vector in the z-direction. Then enforcing that the flow has only an axial velocity component and introducing the gravity function $f(2\pi z/L)$ giving the component of gravity in the axial direction, one arrives at the equations

$$\frac{\partial w}{\partial z} = 0, \tag{2.4}$$

$$\frac{\partial w}{\partial t} + \frac{\partial}{\partial z} \left(\frac{p}{\rho} \right) = \nu \nabla^2 w + \alpha (T - T_0) g f \left(\frac{2\pi z}{L} \right), \tag{2.5}$$

$$\frac{\partial T}{\partial t} + w \frac{\partial T}{\partial z} = \kappa \nabla^2 T, \tag{2.6}$$

Here w is axial velocity and z is the axial direction. It is easily seen by taking the z-derivative of (2.5) that the pressure for the reduced system is independent of x and y.

The equation of continuity implies that $w = w(x, y, t)$. In these equations the Laplacian is the two-dimensional Laplacian with respect to the variables x and y.

https://doi.org/10.1017/S0022112005006361 Published online by Cambridge University Press

Using the variable $\theta = 2\pi z/L$, we can write our boundary conditions as

$$T(x, y, \theta, t) = T(x, y, \theta + 2\pi, t),$$
$$w(x, y, t) = 0 \text{ on } \partial S,$$
$$T(x, y, \theta, t) = T_0 + T_{wall}(\theta) \text{ on } \partial S,$$

where ∂S is the boundary of the cross-section, $r = R$. For the majority of this paper, $R = 1$.

The above set of equations is based on a few approximations. We have assumed that the velocity has only an axial component which is independent of the axial coordinate, and we have ignored the axial components of the Laplacian. We make these assumptions in the case of small aspect ratio (ratio of the cross-sectional radius of the tube to its length). Previous reduced-order models of the thermosyphon have made the same assumption concerning the velocity profile, and they have assumed a particular form for this velocity profile as well, namely that it is parabolic. Our analysis drops this last assumption. The assumption that the velocity is predominantly in the axial direction is a very sound one; the assumption that the profile is independent of the axial coordinate is an approximation, and we believe that in order to have an asymptotic model rather than a heuristic model, this assumption would have to be dropped.

Assuming that our governing equations of motion hold, the flow at any cross-section described by this system will be axisymmetric, until a bifurcation occurs that breaks this symmetry. With this in mind, throughout this paper we assume that the flows at any cross-section are axisymmetric.

We integrate the momentum equation (2.5) over the whole length of the tube, and periodicity in θ causes the pressure gradient to integrate to zero in that direction. We arrive at the equation

$$\frac{\partial w}{\partial t} - g\alpha\phi = \nu\nabla^2 w \tag{2.7}$$

where

$$\phi(x, y, t) = \frac{1}{2\pi}\int_{-\pi}^{\pi} f(\theta)\,(T(x, y, \theta, t) - T_0)\,\mathrm{d}\theta.$$

Similarly if we multiply (2.6) by $f(\theta)$, integrate over the length of the tube, integrate the advective term by parts, and use the periodicity of $f(\theta)$ and T, we arrive at the equation

$$\frac{\partial \phi}{\partial t} - \frac{2\pi}{L}\psi w = \kappa\nabla^2\phi \tag{2.8}$$

where

$$\psi(x, y, t) = \frac{1}{2\pi}\int_{-\pi}^{\pi} f'(\theta)\,(T(x, y, \theta, t) - T_0)\,\mathrm{d}\theta.$$

Finally, if we multiply (2.6) by $f'(\theta)$, integrate over the length of the tube, and integrate the advective term by parts, we arrive at the equation

$$\frac{\partial \psi}{\partial t} + \frac{2\pi}{L}\chi w = \kappa\nabla^2\psi \tag{2.9}$$

where

$$\chi(x, y, t) = -\frac{1}{2\pi}\int_{-\pi}^{\pi} f''(\theta)\,(T(x, y, \theta, t) - T_0)\,\mathrm{d}\theta.$$

https://doi.org/10.1017/S0022112005006361 Published online by Cambridge University Press

Equations (2.7)–(2.9) give us three partial differential equations in the four unknowns $w(x, y, t)$, $\phi(x, y, t)$, $\psi(x, y, t)$, and $\chi(x, y, t)$. In general this system is not a closed system of equations: we could continue multiplying (2.6) by higher derivatives of $f(\theta)$ to get more equations in more unknowns, but the system would not be closed. However, for the case of a circular loop, where $f(\theta) = \sin(\theta)$, we have

$$\phi(x, y, t) = \chi(x, y, t) \text{ for } \quad f(\theta) = \sin(\theta)$$

resulting in a closed system of equations. In the next section we show that for an arbitrary symmetric loop, where $f(-\theta) = -f(\theta)$, the systems governing the onset of convection also close.

We need to supplement our partial differential equations with boundary conditions. These boundary conditions are given by multiplying our exact boundary conditions by 1, $f(\theta)$, $f'(\theta)$, or $f''(\theta)$ and integrating over θ. This leads to the boundary conditions

$$\begin{aligned} w(x, y) &= 0 \text{ on } \partial S, \\ \phi(x, y) &= A_0 \text{ on } \partial S, \\ \psi(x, y) &= A_1 \text{ on } \partial S, \\ \chi(x, y) &= A_2 \text{ on } \partial S, \end{aligned}$$

where A_0 and A_1, and A_2 are defined as

$$\begin{aligned} A_0 &= \frac{1}{2\pi} \int_{-\pi}^{\pi} f(\theta) T_{wall}(\theta) \, \mathrm{d}\theta, \\ A_1 &= \frac{1}{2\pi} \int_{-\pi}^{\pi} f'(\theta) T_{wall}(\theta) \, \mathrm{d}\theta, \\ A_2 &= -\frac{1}{2\pi} \int_{-\pi}^{\pi} f''(\theta) T_{wall}(\theta) \, \mathrm{d}\theta. \end{aligned}$$

For symmetric loops with T_{wall} an even function, $A_0 = A_2 = 0$. For simplicity drop the subscript, denoting $A_1 = A$.

Define the dimensionless variables by $\phi = A\tilde{\phi}$, $\psi = A\tilde{\psi}$, $\chi = A\tilde{\chi}$, $w = (g\alpha R^2 A\kappa/\nu^2)\tilde{w}$, $t = (R^2/\nu)\tilde{t}$, $x = R\tilde{x}$, and $y = R\tilde{y}$, where R is the radius of the cross-section of the loop. Inserting these into (2.7)–(2.9) gives

$$Pr \frac{\partial \tilde{\phi}}{\partial \tilde{t}} - Gr \tilde{\psi} \tilde{w} = \tilde{\nabla}^2 \tilde{\phi}, \tag{2.10}$$

$$Pr \frac{\partial \tilde{\psi}}{\partial \tilde{t}} + Gr \tilde{\chi} \tilde{w} = \tilde{\nabla}^2 \tilde{\psi}, \tag{2.11}$$

$$\frac{\partial \tilde{w}}{\partial \tilde{t}} - Pr \tilde{\phi} = \tilde{\nabla}^2 \tilde{w}, \tag{2.12}$$

where the parameters are the diffusion ratio Pr (Prandtl number), and the control parameter Gr (Grashof number):

$$Pr = \frac{\nu}{\kappa}, \tag{2.13}$$

$$Gr = \frac{Ra}{Pr} = \frac{2\pi g \alpha R^4 A}{\nu^2 L}, \tag{2.14}$$

where $Ra = 2\pi g\alpha R^4 A/\nu\kappa L$ is the Rayleigh number.

For simplicity, we require that ψ has the constant value A at the boundary, so that $\tilde{\psi} = 1$. Throughout the rest of this paper we will drop the tilde notation.

https://doi.org/10.1017/S0022112005006361 Published online by Cambridge University Press

For the majority of this paper we consider the case of a circular loop where $f(\theta) = \sin(\theta)$, and hence $\phi(x, y, t) = \chi(x, y, t)$. The only exception to this will be in the next section where we consider the linear stability of the non-convecting solution. Throughout this paper, we assume that the cross-section is circular and that there is radial symmetry in the solutions.

When analysing circular loops we rewrite the system in vector form as

$$(\boldsymbol{D}\partial_t - \boldsymbol{I}\nabla^2 - \boldsymbol{P})\boldsymbol{u} = GrF(\boldsymbol{u}), \tag{2.15}$$

with

$$\boldsymbol{u} = \begin{pmatrix} \phi \\ \psi \\ w \end{pmatrix} = \begin{pmatrix} u_1 \\ u_2 \\ u_3 \end{pmatrix},$$

$$\boldsymbol{F}(\boldsymbol{u}) = u_3\boldsymbol{M}\boldsymbol{u} = u_3 \begin{bmatrix} 0 & 1 & 0 \\ -1 & 0 & 0 \\ 0 & 0 & 0 \end{bmatrix} \boldsymbol{u}, \quad \boldsymbol{D} = \begin{bmatrix} Pr & 0 & 0 \\ 0 & Pr & 0 \\ 0 & 0 & 1 \end{bmatrix}, \quad \boldsymbol{P} = \begin{bmatrix} 0 & 0 & 0 \\ 0 & 0 & 0 \\ Pr & 0 & 0 \end{bmatrix}.$$

Boundary conditions are given by

$$\boldsymbol{u} = \begin{pmatrix} 0 \\ 1 \\ 0 \end{pmatrix} \text{ on } \partial S. \tag{2.16}$$

The system (2.15) along with the boundary condition (2.16) is the reduced PDE model that is the focus of this study.

Many thermosyphon models begin with a Lorenz-like system. The present model can be further reduced to the ODE Lorenz model by imposing a parabolic profile and integrating around the loop. We present the details of such a reduction in Appendix A.

3. The onset of convection

3.1. *Steady solution and bifurcation point*

We begin by considering the case of the circular loop, where $\phi(x, y, t) = \chi(x, y, t)$, and the equations of motion are governed by the system (2.15) along with its boundary conditions (2.16). This equation has the steady-state solution

$$\boldsymbol{u} = \begin{pmatrix} 0 \\ 1 \\ 0 \end{pmatrix}.$$

To locate the first bifurcation we express the linear problem by an expansion about the steady solution in a neighbourhood of the critical Grashof number, Gr_p, by

$$\boldsymbol{u} = \boldsymbol{u}_0 + \epsilon\boldsymbol{u}_1(r) + O(\epsilon^2),$$

where ϵ measures the projection of the difference between the bifurcated solution and the steady-state solution onto the left critical eigenvector. Since the linearized operator, along with null boundary conditions and the inner product $\langle \boldsymbol{u}, \hat{\boldsymbol{u}} \rangle = \int_0^1 (Pr\phi\hat{\phi} + \psi\hat{\psi} + Gr_p w\hat{w})r \, \mathrm{d}r$ is self-adjoint, the temporal spectrum is real and the principle of exchange of stability holds at the bifurcation point. As with the classical Rayleigh–Bénard problem, we can determine the critical Grashof number by solving a linear eigenvalue

https://doi.org/10.1017/S0022112005006361 Published online by Cambridge University Press

problem. Specifically, the system for $\boldsymbol{u}_1$ can be written as

$$\nabla^2 \boldsymbol{u}_1 + \begin{pmatrix} 0 & 0 & Gr_p \\ 0 & 0 & 0 \\ Pr & 0 & 0 \end{pmatrix} \boldsymbol{u}_1 = 0$$

along with null boundary conditions on the perturbation variables.

The equation for ψ_1 decouples to give

$$\nabla^2 \psi_1 = 0,$$
$$\psi_1 = 0 \text{ on } \partial S,$$

which has solution

$$\psi_1 = 0.$$

The eigenvalue problem for variables ϕ_1 and w_1 is given by

$$\nabla^2 \begin{pmatrix} \phi_1 \\ w_1 \end{pmatrix} = \begin{pmatrix} 0 & -Gr_p \\ -Pr & 0 \end{pmatrix} \begin{pmatrix} \phi_1 \\ w_1 \end{pmatrix}, \tag{3.1}$$

$$\begin{pmatrix} \phi_1 \\ w_1 \end{pmatrix} = 0 \text{ on } \partial S. \tag{3.2}$$

To show that the only possible eigenfunctions are Bessel functions, define

$$\lambda = \sqrt{Gr_p Pr}.$$

Then ϕ_1 must satisfy the equation

$$\nabla^4 \phi_1 - \lambda^2 \phi_1 = 0,$$

which can be written as

$$\nabla^2 \Phi - \lambda \Phi = 0, \tag{3.3}$$

where

$$\Phi = \nabla^2 \phi_1 + \lambda \phi_1.$$

Since ϕ_1 and w vanish on the boundary, ϕ_1 and $\nabla^2 \phi_1$ must vanish on the boundary, and hence Φ must vanish on the boundary. It follows that we have the boundary condition

$$\Phi = 0 \text{ on } \partial S. \tag{3.4}$$

Notice that we have defined λ as a positive number, and so the system (3.3) and (3.4) has only the trivial solution. Then Φ is identically equal to zero. This implies that we have the equation

$$\nabla^2 \phi_1 + \lambda \phi_1 = 0,$$
$$\phi_1 = 0 \text{ on } \partial S.$$

Assuming that ϕ_1 has the form

$$\phi_1(r, \theta) = \mathrm{e}^{\mathrm{i}n\theta} q(r)$$

we see that $q(r)$ must satisfy the eigenvalue problem

$$\frac{1}{r} \frac{\mathrm{d}}{\mathrm{d}r} \left(r \frac{\mathrm{d}q}{\mathrm{d}r} \right) - q \frac{n^2}{r^2} + \lambda q = 0,$$
$$q(1) = 0.$$

https://doi.org/10.1017/S0022112005006361 Published online by Cambridge University Press

The general solution to this equation that is not singular at the origin is given by

$$q(r) = K J_n(\sqrt{\lambda} r)$$

where J_n is the nth Bessel function. This shows that the system (3.1)–(3.2) has eigenfunctions of the form

$$\begin{pmatrix} \phi_{1,n} \\ w_{1,n} \end{pmatrix} = \begin{pmatrix} c_1 \\ c_2 \end{pmatrix} J_n(\gamma_{nm} r)$$

where

$$J_n(\gamma_{nm}) = 0.$$

Then

$$-\gamma_{nm}^2 \begin{pmatrix} c_1 \\ c_2 \end{pmatrix} = \begin{pmatrix} 0 & -Gr_p \\ -Pr & 0 \end{pmatrix} \begin{pmatrix} c_1 \\ c_2 \end{pmatrix},$$

and satisfying the condition

$$\begin{vmatrix} \gamma_{mn}^2 & -Gr_p \\ -Pr & \gamma_{mn}^2 \end{vmatrix} = 0$$

gives the critical parameter value for the pitchfork bifurcation,

$$Gr_p = \frac{\gamma_{mn}^4}{Pr}.$$

The minimum over all m and n is given by $Gr_p = \gamma_{01}$, the first zero of the zero-order Bessel function. Note that this result correlates to the pitchfork bifurcation one finds in the Lorenz equations, where the pitchfork bifurcation is a function of the Rayleigh number (Tritton 1988). Because $Gr = Ra/Pr$, this result can be written $Ra_p = \gamma_{01}^4$. That this critical value is independent of Prandtl number is characteristic of this type of flow.

The eigenvector is given by

$$\begin{pmatrix} c_1 \\ c_2 \end{pmatrix} = \begin{pmatrix} \gamma_{01}^2 \\ Pr \end{pmatrix},$$

and so the first-order solution is

$$\boldsymbol{u}_1 = a_1 \begin{pmatrix} \gamma_{01}^2 J_0(\gamma_{01} r) \\ 0 \\ Pr J_0(\gamma_{01} r) \end{pmatrix},$$

where a_1 is constant. Because at the bifurcation point the eigenfunction has radial symmetry, and the bifurcation was not symmetry-breaking, then the bifurcated solution has the same symmetry.

We now briefly comment on the linear stability of the non-convecting state for arbitrary symmetric loops. By a symmetrical loop we mean one that has reflectional symmetry about a plane P containing a vertical line. For loops of this form we have $f(-\theta) = -f(\theta)$, and hence $f''(-\theta) = -f''(\theta)$. Before the onset of convection, the flow will have reflectional symmetry about the plane P. For this reason we know that for this solution $\phi_0 = \chi_0 = 0$. In this general case, the equation for ψ is coupled to χ (rather than ϕ through the term $w\chi$). However, in the linear theory this is a second-order term, since $\chi_0 = 0$. It follows that in the general case the linear theory applies, with the constant A being determined by the general expression for $f(\theta)$ rather than using $f(\theta) = \sin(\theta)$.

3.2. *Supercritical pitchfork bifurcation and global stability*

The global stability of this trivial branch is proved in Appendix B.

https://doi.org/10.1017/S0022112005006361 Published online by Cambridge University Press

There is a limit of the parameters (Grashof number and Prandtl number) below which any perturbation will settle to the trivial solution. This limit is identical to the pitchfork bifurcation point found above. Because the trivial branch is globally stable up to the pitchfork bifurcation point, this proves that the pitchfork bifurcation is supercritical. The global stability boundary is also important in that it limits the range of the secondary bifurcations. This will be discussed further in § 4.

The proof of global stability proceeds as follows. First we define an energy function that depends on a parameter λ. The rate of change of energy can be maximized by a function $Gr(\lambda)$ of the Grashof number, and each value of λ corresponds to a different energy rate. We show that this rate of change of energy is always negative. Then maximizing this function of Grashof number over all values of λ, we find the optimal energy function, that is, the one that gives the largest value of Gr for which a decaying energy rate can be guaranteed. This value of Gr is the global stability limit, and corresponds to the pitchfork bifurcation point. Details are provided in Appendix B. We note that a similar result occurs in the Boussinesq equations of the Rayleigh–Bénard problem, and the global stability of the trivial branch there is proved by Joseph (1976).

3.3. *Numerical results*

The critical Grashof number is found to be $Gr_p = \gamma_{01}^4/Pr$, or $Ra_p = \gamma_{01}^4$. Using the spectral code described in § 5, we find that the onset of convection agrees with this analytic result to machine precision. Similarly, results with the full three-dimensional simulation using MPSalsa, also discussed in § 5, converge toward the asymptotic result with mesh refinement. The close agreement of the three independent methods of locating the onset of convection lend validation to the assumptions we have made in deriving the reduced PDE model given by (2.15) and (2.16).

This asymptotic result is also in qualitative agreement with models that use the Lorenz equations, where the initial bifurcation point is at the constant $R = 1$ (see Appendix A). Using the Lorenz equations (A 1), with parameters based on our particular derivation, we find that the system will become convective at $Ra = 64$; in fact, from our previous analysis, it is seen to become unstable at $Ra = \gamma_{01}^4 \approx 33.44$, so a thermosyphon model using our derivation of the Lorenz equations will overpredict the region where the trivial solution is stable.

Table 1 illustrates the location of the eigenvalues found with the spectral code. Notice the convergence of the eigenvalues with increased resolution. For a variety of Gr, 32 modes suffice to find the eigenvalue to 8 significant figures. Figures 2 and 3 illustrate the location of eigenvalues in the complex plane for various Grashof numbers for $Pr = 7$, computed with the spectral eigenvalue code. Table 2 compares results for the most unstable eigenvalue computed using the finite element code, MPSalsa with results computed using the spectral eigenvalue code. This demonstrates that the full three-dimensional simulation requires a quite refined mesh to achieve the accuracy of the spectral method, though a coarser mesh is sufficient to capture the transition within a given range of Grashof values. Details of the numerical methods of each code are presented in § 5.

4. Stability and bifurcation of the convective branch

In this section, we will examine the stability of the convective branch and analyse the Hopf bifurcation. We introduce a method that allows us to obtain the criticality of this Hopf bifurcation solution.

https://doi.org/10.1017/S0022112005006361 Published online by Cambridge University Press

N	λ_1	λ_2	λ_3
$Pr = 7,\ Gr = 4;\ Gr_p = 4.78$			
16	−0.11986932	−0.82616942	−4.20077833
32	−0.11986928	−0.82616942	−4.20077531
64	−0.11986928	−0.82616942	−4.20077531
$Pr = 7,\ Gr = 5;\ Gr_p = 4.78$			
16	$3.3436286822 \times 10^{-2}$	−0.82616942	−4.16298621
32	$3.3436286827 \times 10^{-2}$	−0.82616942	−4.16298317
64	$3.3436286827 \times 10^{-2}$	−0.82616942	−4.16298317
$Pr = 20,\ Gr = 1;\ Gr_p = 1.67$			
16	−0.11280433	−.28915930	−1.48906023
32	−0.11280433	−.28915930	−1.48905918
64	−0.11280433	−.28915930	−1.48905918
$Pr = 20,\ Gr = 2;\ Gr_p = 1.67$			
16	$5.35008552 \times 10^{-2}$	−0.28915930	−1.45463818
32	$5.35008552 \times 10^{-2}$	−0.28915930	−1.45463711
64	$5.35008552 \times 10^{-2}$	−0.28915930	−1.45463711

TABLE 1. The first three eigenvalues of flow in a thermosyphon for the trivial branch. N = number of spectral modes. Note that the trivial flow becomes unstable at $Gr = \gamma_{01}^4/Pr$. Note also that λ_2 depends only on the ψ component of temperature and so is independent of Gr.

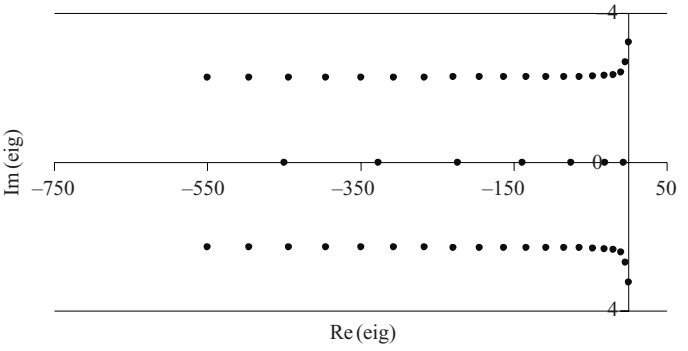


FIGURE 2. Eigenvalues at $Pr = 7, Gr = 50$.

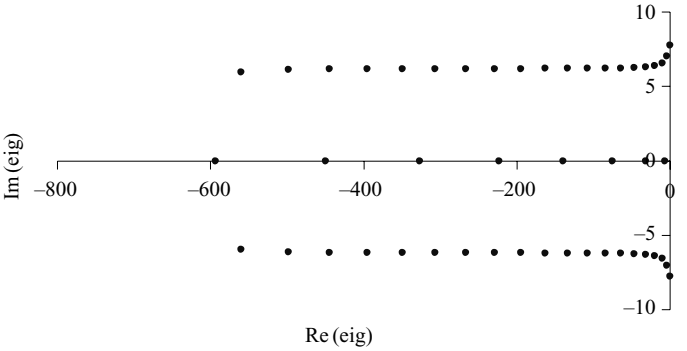


FIGURE 3. Eigenvalues at $Pr = 7, Gr = 300$ with $N = 32$.

https://doi.org/10.1017/S0022112005006361 Published online by Cambridge University Press

N	$Gr = 30$	$Gr = 32.5$	$Gr = 35$	$Gr = 37.5$
$Pr = 1$; $Gr_p = 33.44$				
20	−0.758	−0.533	−0.316	−0.108
40	−0.389	−0.163	0.054	0.264
80	−0.303	−0.078	0.139	0.348
spectral	−0.306	−0.082	0.133	0.341
asymptotic	−0.306	−0.082	0.133	0.341
N	$Gr = 4.29$	$Gr = 4.64$	$Gr = 5$	$Gr = 5.36$
$Pr = 7$; $Gr_p = 4.78$				
20	−0.176	−0.123	−0.0705	−0.0189
40	−0.0967	−0.0370	0.0171	0.0704
80	−0.0713	−0.0158	0.0387	0.0923
spectral	−0.0753	−0.0205	0.03334	0.0865
asymptotic	−0.0753	−0.0205	0.03334	0.0865

TABLE 2. The first eigenvalue of the trivial branch for flow in a thermosyphon computed with MPSalsa with $R_T = 1$, $R_H = 10$, and $N^2/16 \times (N + N/20)$ uniform mesh. The spectral result at resolution 32 modes corresponds to the eigenvalue computed directly from the asymptotic model.

4.1. *Convective solution and bifurcation point*

For $Gr > Gr_p$, we compute the convective solution to the system (2.15) and (2.16) numerically using the spectral code described in § 5. Solution profiles computed with this code are given in figures 8–10 in § 6.

The system resulting from linearizing about the convective branch is given by (see Appendix C)

$$(\boldsymbol{D}\partial_t - \boldsymbol{I}\nabla^2 - \boldsymbol{P})\boldsymbol{u}_1 = Gr_h J_0 \boldsymbol{u}_1. \tag{4.1}$$

This system can be cast as a generalized eigenvalue problem to determine the critical Grashof number, Gr_h, indicating where the convective solution loses its stability. This is found to occur through a Hopf bifurcation. See figure 11 in § 6 for the numerically computed critical Grashof number as it depends on Prandtl number. In table 3 we report eigenvalues of the convective branch obtained using the spectral code. We note that attempts to locate the Hopf bifurcation using MPSalsa have as yet been unsuccessful, due to the large systems that result from the fine mesh discretizations necessary to capture the dynamics of the flow at these high Grashof and Prandtl numbers. We view this as confirmation that our strategy of employing a highly accurate reduced PDE model easily discretized by a spectral method is necessary in conducting a stability and bifurcation analysis of the thermosyphon problem in the parameter range exhibiting periodic behaviour.

4.2. *Criticality of the bifurcating solution*

We use a weakly nonlinear stability analysis to examine the solution in a neighbourhood of the steady-state solution. Additionally, we employ a multiple-time-scale analysis, allowing $\tau = \epsilon^2 t$, where $\epsilon = \sqrt{|Gr - Gr_h|}$ with Gr_h the bifurcation point so that $Gr = Gr_h + j\epsilon^2$ with $j = \pm 1$ according to whether we consider values of Gr above or below the bifurcation point. The base state is time independent, and in this analysis one considers perturbations that can depend on the 'slow' time, τ. We make a further rescaling to the time variable so that the bifurcating periodic solution has

https://doi.org/10.1017/S0022112005006361 Published online by Cambridge University Press

N	λ_1	λ_2	λ_3
$Gr = 10$			
16	$-0.38966583 \pm 1.06623072$i	$-4.22920743 \pm 0.83528015$i	-6.71435768
32	$-0.38967750 \pm 1.06625057$i	$-4.22924245 \pm 0.83529406$i	-6.71433609
64	$-0.38967750 \pm 1.06625057$i	$-4.22924245 \pm 0.83529406$i	-6.71433609
$Gr = 50$			
16	$-0.29153807 \pm 3.22110087$i	$-4.08359747 \pm 2.68818657$i	-7.10593143
32	$-0.29158500 \pm 3.22112920$i	$-4.08324280 \pm 2.68805007$i	-7.10590921
64	$-0.29158500 \pm 3.22112920$i	$-4.08324280 \pm 2.68805007$i	-7.10590921
$Gr = 300$			
16	$-2.86 \times 10^{-2} \pm 7.76286427$i	$-3.98176664 \pm 7.04824907$i	-7.06274178
32	$-2.74 \times 10^{-2} \pm 7.76272788$i	$-3.98493589 \pm 7.05070856$i	-7.06544438
64	$-2.74 \times 10^{-2} \pm 7.76272788$i	$-3.98493592 \pm 7.05070859$i	-7.06544440
$Gr = 350$			
16	$-2.30 \times 10^{-3} \pm 8.34640116$i	$-3.95978468 \pm 7.60465151$i	-7.03438673
32	$-8.37 \times 10^{-4} \pm 8.34580017$i	$-3.96462820 \pm 7.60592416$i	-7.03555062
64	$-8.37 \times 10^{-4} \pm 8.34580016$i	$-3.96462826 \pm 7.60592417$i	-7.03555065

TABLE 3. The first three eigenvalues of the convective branch for flow in a thermosyphon with $Pr = 7.0$ $N =$ number of modes.

frequency 1 with the substitution $s = \omega t$. The bifurcation frequency will enter the system explicitly.

Assuming completeness of the eigenfunctions of the linearized system, a solution can be expanded:

$$\boldsymbol{u}(r, t, \tau) = \sum_i a_i(\tau) \mathrm{e}^{\lambda_i t} \boldsymbol{u}_i(r) + \text{c.c.},$$

where c.c. denotes the complex conjugate. The goal is to identify the nonlinear behaviour of the solution near the bifurcation point.

Expand the solution

$$\boldsymbol{u} = \boldsymbol{u}_0(r) + \epsilon \boldsymbol{u}_1(s, r) + \epsilon \boldsymbol{u}_2(s, r) + O(\epsilon^3).$$

Expand the frequency as

$$\omega = \omega_0 + \epsilon \omega_1 + \epsilon^2 \omega_2 + O(\epsilon^3).$$

Standard Hopf bifurcation theory gives that $\omega_1 = 0$. Consider the expansion in a neighbourhood of the critical Grashof number, $Gr = Gr_h$. See Appendix C for analysis of the resulting system under this expansion.

4.3. *A numerical scheme to extract Landau coefficients*

We can continue the above analysis to characterize the bifurcation. At order ϵ^3 we arrive at a Landau equation

$$\frac{\mathrm{d}a(\tau)}{\mathrm{d}\tau} = j\alpha a(\tau) + \beta |a(\tau)|^2 a(\tau) \tag{4.2}$$

where the computation of the constants $j = \pm 1$ and α and β can be carried out by standard asymptotic methods as shown in Appendix C. As an alternative to computing the coefficients explicitly, we can use the following numerical scheme to extract the Landau coefficients.

https://doi.org/10.1017/S0022112005006361 Published online by Cambridge University Press

It is the signs of the real parts of α and β in (4.2) that determine whether the bifurcation is sub- or supercritical. In particular, when $j\alpha/\beta > 0$, the bifurcation is subcritical, and when $j\alpha/\beta < 0$, the bifurcation is supercritical. Writing $a(\tau)$ in polar form as $\rho(\tau)e^{i\theta(\tau)}$ and α and β in complex form as $\alpha_r + i\alpha_i$, $\beta_r + i\beta_i$, respectively, gives

$$\frac{d\rho}{d\tau} = j\alpha_r\rho + \beta_r\rho^3,$$
$$\frac{d\theta}{d\tau} = j\alpha_i + \beta_i\rho^2.$$

The extraction procedure is as follows. Compute the time integration of the full equations, with an initial value of $\boldsymbol{u}_0 + \epsilon\boldsymbol{A}_{1i}$, where $\boldsymbol{u}_0$ is the convective solution at the bifurcation point and $\boldsymbol{A}_{1i}$ is the imaginary part of the eigenvector associated with the leading eigenvalue at the bifurcation point. Note that this is just a particular choice of constants c_r and c_i in the $O(\epsilon)$ solution

$$(c_r + ic_i)e^{i\omega_0 t}(\boldsymbol{A}_{1r} + i\boldsymbol{A}_{1i}) + \text{c.c.}$$

At every time t, compute the solution $\boldsymbol{\Phi}(r, t)$. The solution must take the form

$$\boldsymbol{\Phi}(r, t, \tau) = \boldsymbol{u}_0 + \epsilon(a(\tau)(\boldsymbol{A}_{1r} + i\boldsymbol{A}_{1i})e^{i\omega_0 t} + \text{c.c. }) + (\text{exponentially decaying modes}).$$

We use this equation to extract the values $a(\tau)$, given $\boldsymbol{A}_{1r}$, $\boldsymbol{A}_{1i}$, and ω_0. In terms of ρ and θ, we have the equation

$$\frac{\boldsymbol{\Phi}(r, t, \tau) - \boldsymbol{u}_0}{\epsilon}$$
$$= 2((\rho\cos\theta\boldsymbol{A}_{1r} - \rho\sin\theta\boldsymbol{A}_{1i})\cos(\omega_0 t) - (\rho\cos\theta\boldsymbol{A}_{1i} + \rho\sin\theta\boldsymbol{A}_{1r})\sin(\omega_0 t)).$$

Integrating $(\boldsymbol{\Phi} - \boldsymbol{u}_0)/\epsilon$ over a period against $\cos(\omega_0 t)$ and $\sin(\omega_0 t)$ respectively gives $2(\rho\cos\theta\boldsymbol{A}_{1r} - \rho\sin\theta\boldsymbol{A}_{1i})$ and $-2(\rho\cos\theta\boldsymbol{A}_{1i} + \rho\sin\theta\boldsymbol{A}_{1r})$. Solving the resulting system of two equations in two unknowns to find $\rho\cos\theta$ and $\rho\sin\theta$ at each point t_n, $n = 1, 2, 3, \ldots$ yields an n-vector of sample points. Extract $\rho_n = \rho(t_n)$ from these and formulate the least-squares problem

$$\frac{d\rho_n}{d\tau} = j\alpha_r\rho_n + \beta_r\rho_n^3$$

and solve for the constants α_r and β_r. We approximate

$$\frac{d\rho}{d\tau}(t_n) = \frac{\rho(t_{n+1}) - \rho(t_{n-1})}{\epsilon^2 2\pi/\omega_0} + O(\epsilon^4).$$

(See Bergeron *et al.* 2000 for a discussion of the use of a similar method of extracting Landau coefficients.)

Table 4 demonstrates the consistency of the extracted coefficients with mode resolution. Simple linear analysis will give an estimate of the coefficient α_r. In table 5 we compare this linear estimate with the extracted coefficient and notice the close agreement.

Results from running this extraction procedure at different Prandtl numbers for various Grashof numbers are also given in table 5. Solutions evolve for 10 periods before data are collected (the time step used is 10^{-4}) to allow the next most unstable mode to decay. Notice the good agreement between the linear analysis and the extracted linear coefficient α. (The formula for computing $d\rho/d\tau$ is second order, explaining the error present in calculating the linear coefficients.)

At Prandtl number 18.5 the bifurcation transitions from sub- to supercritical. Figure 4 shows the ratio of $j\alpha/\beta$ for various Prandtl numbers for Gr approximately

https://doi.org/10.1017/S0022112005006361 Published online by Cambridge University Press

N	extract α_r	extract β_r
$Pr = 7$ $Gr = 345$		
32	-4.80×10^{-4}	0.738×10^{-4}
64	-4.80×10^{-4}	0.809×10^{-4}
128	-4.80×10^{-4}	0.702×10^{-4}
$Pr = 15$ $Gr = 196$		
32	-6.33×10^{-4}	0.197×10^{-4}
64	-6.33×10^{-4}	0.196×10^{-4}
128	-6.33×10^{-4}	0.199×10^{-4}
$Pr = 20$ $Gr = 223$		
32	-4.01×10^{-4}	-0.065×10^{-4}
64	-4.01×10^{-4}	-0.069×10^{-4}
128	-4.00×10^{-4}	-0.073×10^{-4}

TABLE 4. Landau coefficients as computed for various mode discretizations N.

Gr	linear α_r	extract α_r	extract β_r
$Pr = 7$ $Gr_h = 351.7679$			
345.0, $j = -1$	-4.80×10^{-4}	-4.80×10^{-4}	0.738×10^{-4}
358.0, $j = +1$	-4.68×10^{-4}	-4.67×10^{-4}	-0.843×10^{-4}
$Pr = 15$ $Gr_h = 200.6050$			
196.0, $j = -1$	-6.33×10^{-4}	-6.33×10^{-4}	0.197×10^{-4}
205.0, $j = +1$	-6.18×10^{-4}	-6.18×10^{-4}	-0.209×10^{-4}
$Pr = 20$ $Gr_h = 227.9197$			
223.0, $j = -1$	-4.00×10^{-4}	-4.01×10^{-4}	-0.065×10^{-4}
233.0, $j = +1$	-3.91×10^{-4}	-3.91×10^{-4}	0.080×10^{-4}

TABLE 5. Landau coefficients for the PDE system with $N = 32$.

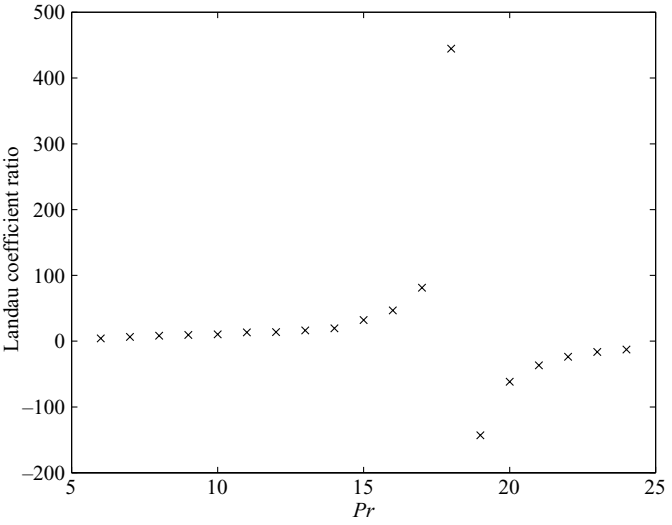


FIGURE 4. The ratio of Landau coefficients $j\alpha/\beta$ for the PDE model indicating the criticality of the Hopf bifurcation.

https://doi.org/10.1017/S0022112005006361 Published online by Cambridge University Press

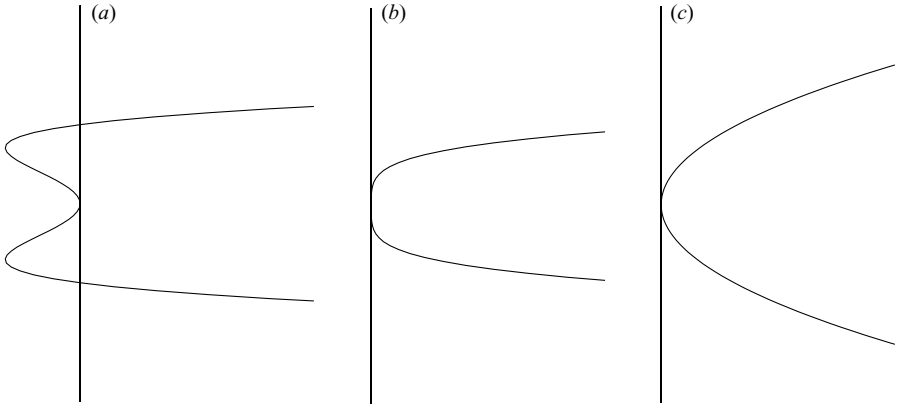


FIGURE 5. Plots of solution vs. Gr_c for (*a*) $Pr < Pr_c$, (*b*) $Pr = Pr_c$, (*c*) $Pr > Pr_c$, respectively.

2% below ($j = -1$) and 2% above ($j = +1$) Gr_c. From the Hopf bifurcation theorem (Glendinning 1994), when this ratio is positive the bifurcation is subcritical and when it is negative the bifurcation is supercritical. While the Lorenz equations do predict a supercritical Hopf bifurcation, they predict the change at a much higher Prandtl number (on the order of $P = 200$ (Tritton 1988)). The difference between the present model and the Lorenz model is significant in this respect. Note that P corresponds directly to Pr (see Appendix A), and experimental verification is feasible.

4.4. *The supercritical Hopf bifurcation*

This model captures periodic behaviour of the flow in the thermosyphon in a parameter value range that is not found in Lorenz-type models, specifically the change from a sub- to supercritical Hopf bifurcation at a Prandtl number of 18.5. This is a significant difference between the models and is evidence that, in particular for flows with Pr greater than 18.5, the reduction to the Lorenz equations is not an accurate model of the flow.

The point (Pr_c, Gr_c) is the most interesting point in parameter space. Here the branching becomes singular, with a Landau equation of the form

$$\frac{\mathrm{d}a}{\mathrm{d}\tau} = \alpha_1 a + \alpha_5 a^5.$$

In the vicinity of this critical point, the equation is of the form

$$\frac{\mathrm{d}a}{\mathrm{d}\tau} = \alpha_1 a + \alpha_3 a^3 + \alpha_5 a^5,$$

where α_3 is very small; this corresponds to the first sketch in figure 5. Figure 5 illustrates the various bifurcation diagrams in the neighbourhood of this critical Prandtl number. For values of Pr just below Pr_c, there is a subcritical bifurcation. This bifurcation must turn around, because of the global stability limit, discussed in § 3 and Appendix B. At Pr_c, the structure is quartic. At $Pr > Pr_c$, the bifurcation is supercritical.

4.5. *Turbulence*

At Grashof and Prandtl numbers of practical interest, the flow in a thermosyphon is laminar. It is known that the chaotic solutions to the Lorenz equations correspond to

https://doi.org/10.1017/S0022112005006361 Published online by Cambridge University Press

Pr	Gr	ω	$w(0)$	$\frac{2\pi}{\omega}$	$\frac{2\pi Pr}{wGr}$
7	351.7679	8.3657	0.1541	0.751	0.812
12	205.1804	5.1394	0.2641	1.22	1.39
15	200.6050	4.6035	0.2956	1.37	1.59
25	299.6914	4.4099	0.3092	1.43	1.70

TABLE 6. Estimation of the time it takes for the fluid to circulate around the loop.

chaotic fluctuations of the fluid as a whole, rather than small-scale turbulent effects. Thus when chaotic motion is seen, it is laminar chaos. See Tritton (1988) for a discussion of turbulence in the Lorenz model.

Creveling *et al.* (1975) performed experiments on flow in a closed-loop thermosyphon and estimated that the flow becomes turbulent at a Reynolds number of approximately 1500. In the variables used in this paper, $Re = 2Grw/(\sigma Pr)$, where w is the dimensionless velocity. It is interesting to note that for a very narrow tube, the flow will be turbulent. In the range of Prandtl and Grashof numbers used in the present work, Gr/Pr is of order 10 and w is of order 0.1. Then the model is valid for laminar flow for an aspect ratio of order 0.01.

4.6. *Flow oscillations*

Consider flow at the Hopf bifurcation point, where the linear stability analysis finds oscillatory flow. As an example case, at the onset of the Hopf bifurcation, $Pr = 7.0$, $Gr = 351.8$, the frequency of the oscillation is $\omega = 8.365$. Taking the velocity at the centre of the profile, $w = 0.154$, estimate the time it takes for the fluid to circulate once around a loop of circumference L by $t = L/w$. Relating these quantities through the dimensionless variables yields $t = 2\pi Pr/wGr = 0.812$. Using the relationship that a period is $2\pi/\omega$ gives $t = 0.751$. The time it takes the fluid to circulate around the loop is roughly equal to a period of the oscillations. This is in agreement with other studies Greif, Zvirin & Mertol 1979). Results for various Prandtl numbers are reported in table 6.

5. Numerical analysis

5.1. *The spectral code*

We numerically compute the solution to the system (2.10)–(2.12) at given Pr and Gr. The primary method of discretization is the pseudospectral method, briefly described below. More complete discussion can be found, for example, in the works of Gottlieb & Orszag (1977), Fornberg (1998), and Canuto *et al.* (1988).

Following the notation of Gottlieb & Orszag, for each t, $\boldsymbol{u}(x,t)$ is an element of a Hilbert Space H with an inner product and a norm. For each $t > 0$, $\boldsymbol{u}(x,t)$ is a member of the subspace B of H where functions in the subspace satisfy the boundary conditions of the problem.

In this work we expand the solution

$$\boldsymbol{u}(x) = \sum_{m=0}^{M} a_m T_m(x)$$

where

$$T_m(x) = \cos(m \arccos(x))$$

https://doi.org/10.1017/S0022112005006361 Published online by Cambridge University Press

are the Chebyshev functions. One obtains the expansion coefficients

$$a_n = \frac{2}{c_n} \int_{-1}^{1} u(x) T_m(x) (1-x)^{-1/2} \, \mathrm{d}x$$

with $c_0 = 2, c_m = 1, m \geqslant 1$.

The method used here is an integration-preconditioned spectral τ (pseudospectral) method. In this method, the expansion functions are not required to satisfy the boundary constraints. Rather, the boundary constraints are imposed as conditions for determining the expansion coefficients, and we make the residual zero at as many spatial points as possible.

This code uses the Gauss–Lobatto points, $x_j = \cos(\pi j/M)$, and so the Chebyshev expansion is a cosine expansion for which one can use a fast Fourier transform.

We will discuss two particular aspects of this numerical method: the preconditioning by an integral operator and the boundary constraints. The derivative operator is an ill-conditioned triangular matrix, whereas the integration operator is a banded matrix. Then preconditioning the system by the appropriate order-n integration operator results in a favourably conditioned system. The first n rows of the system become zero, and one can replace these with row vectors associated with the boundary constraints. See Coutsias *et al.* (1995) for further details.

To investigate the transient and steady-state behaviour of the system, we implemented a time-dependent solver. The spatial component is discretized using the pseudospectral method and the temporal component, as is customary in the use of spectral methods to solve PDEs, using a finite difference method.

Consider the equation

$$Pr \frac{\partial u}{\partial t} = Lu + f(r,t) + N(u)$$

where $f(r,t)$ is a forcing term and $N(u)$ is a nonlinear term. This code computes Lu and $f(r,t)$ implicitly and $N(u)$ explicitly. Discussion of the use of implicit-explicit schemes is found in the paper by Ascher, Ruuth & Wetton (1995).

As an alternative means to find the steady-state flow, we have developed a Newton code that directly finds a steady solution. This code has the advantage over the time-dependent solver of quickly locating a steady state, and the matrices used in the Newton code are the same as those used in finding the eigenvalues of the system. The Newton code provides confirmation of steady-state results obtained via the time-dependent code. In the time-dependent code we used time steps between 10^{-2} and 10^{-4}.

5.2. *Three-dimensional calculations with MPSalsa*

We will discuss the numerical methods used by MPSalsa to locate steady-state solutions of (2.1)–(2.3), the formulation of the eigenvalue problem and the Cayley transform method, and the numerical solution of the eigenvalue problem.

A full description of the numerical methods in MPSalsa used to locate steady-state solutions of (2.1)–(2.3) is available in Shadid (1999) and the references listed therein. A brief overview is presented in this section.

A mesh of quadrilaterals for two-dimensional problems and hexahedra for three-dimensional problems is generated to cover the domain. Although the code allows for general unstructured meshes, the simple geometry of the present problem allows the easy use of structured meshes. For parallel runs, the mesh is partitioned using the Chaco code (Hendrickson & Leland 1995) in a way that will distribute work evenly

https://doi.org/10.1017/S0022112005006361 Published online by Cambridge University Press

while minimizing communication costs between processors. A Galerkin/least-squares finite element method (GLS-FEM) (Hughes, Franca & Hulbert 1989) is used to discretize the time-invariant versions of the governing partial differential equations (2.1)–(2.3) into a set of nonlinear algebraic equations. This formulation includes a pressure stabilization term so that the velocity components, temperature and pressure fields can all be represented with equal-order nodal basis functions. GLS-FEM is a consistent stabilized scheme because when the exact solution is inserted, the Boussinesq equations are satisfied exactly. The code uses bilinear and trilinear nodal elements for two- and three-dimensional problems, respectively.

Discretization of (2.1)–(2.3) results in the matrix equation

$$\begin{pmatrix} \boldsymbol{M} & 0 \\ \boldsymbol{N} & 0 \end{pmatrix} \begin{bmatrix} \dot{\boldsymbol{u}} \\ \dot{\boldsymbol{p}} \end{bmatrix} + \begin{pmatrix} \boldsymbol{K}_{u,T} + \boldsymbol{C}(\boldsymbol{u}) & -\boldsymbol{D} \\ \boldsymbol{D}^T + \boldsymbol{G} & \boldsymbol{K}_p \end{pmatrix} \begin{bmatrix} \boldsymbol{u} \\ \boldsymbol{p} \end{bmatrix} - \begin{bmatrix} \boldsymbol{g} \\ \boldsymbol{h} \end{bmatrix} = \begin{bmatrix} \boldsymbol{0} \\ \boldsymbol{0} \end{bmatrix} \tag{5.1}$$

where u is the vector of fluid velocity components and temperature unknowns, p is the pressure, $\boldsymbol{M}$ is the symmetric positive definite matrix of the overlaps of the finite element basis functions, $\boldsymbol{K}_{u,T}$ is the stiffness matrix associated with velocity and temperature, $\boldsymbol{C}(\boldsymbol{u})$ is the nonlinear convection, $\boldsymbol{D}$ is the discrete (weak) gradient, $\boldsymbol{D}^T$ is the discrete (weak) divergence operator and $\boldsymbol{K}_p$ is the stiffness matrix for the pressure. $\boldsymbol{G}, \boldsymbol{K}_p, \boldsymbol{N}$ are stabilization terms arising from the GLS-FEM. The vectors g and h denote terms due to boundary conditions and the Boussinesq approximation.

The resulting nonlinear algebraic equations arising from setting the time-derivative terms to zero are solved using a fully coupled Newton–Raphson method (Shadid, Tuminaro & Walker 1997). An analytic Jacobian matrix for the entire system is calculated and stored in a sparse matrix storage format. At each Newton–Raphson iteration, the linear system is solved using the Aztec package (Tuminaro *et al.* 1999) of parallel preconditioned Krylov iterative solvers. The accuracy of the steady-state solution is set by the following stopping criterion:

$$\left(\frac{1}{N} \sum_{i=1}^{N} \left(\frac{|\delta_i|}{\epsilon_R |x_i| + \epsilon_A} \right)^2 \right)^{1/2} < 1.0,$$

where ϵ_R and ϵ_A are the relative and absolute tolerances desired, δ_i is the update for the unknown x_i and N is the total number of unknowns. We use relative and absolute tolerances of 10^{-5} and 10^{-8}, respectively, for this study. In Aztec the code exclusively uses an unrestarted GMRES iteration with a non-overlapping Schwarz preconditioner where an ILU preconditioner is used on each sub-domain (each processor contains one sub-domain). These methods enable rapid convergence to both stable and unstable steady-state solutions. The scalability of these methods to large system sizes and numbers of processors is demonstrated by the solution of a 16 million unknown model on 2048 processors (Burroughs *et al.* 2001).

The GLS-FEM results in a spatial discretization of the Navier–Stokes equations with the Boussinesq approximation. This leads to a finite-dimensional system of differential algebraic equations of the form

$$\boldsymbol{B}\dot{\boldsymbol{x}} = \boldsymbol{F}(\boldsymbol{x}), \qquad \boldsymbol{x}(0) = \boldsymbol{x}_0, \tag{5.2}$$

where the matrix $\boldsymbol{B}$ is singular (due to the divergence-free constraint) and $\boldsymbol{x}$ is a vector containing the nodal values of the velocities, temperature and pressure at the nodes of the finite element mesh. Because of the stabilization terms in the GLS discretization,

https://doi.org/10.1017/S0022112005006361 Published online by Cambridge University Press

$\boldsymbol{B}$, the matrix associated with the time-derivative term in (5.1) is a non-symmetric matrix.

We solve the generalized eigenvalue problem

$$\lambda \boldsymbol{B} z = \boldsymbol{J}(\boldsymbol{x}_s) z \equiv \boldsymbol{J} z. \tag{5.3}$$

that arises from the linearisation of (5.2) about the steady state. The matrix $\boldsymbol{J}(\boldsymbol{x}_s)$ is the Jacobian of $\boldsymbol{F}(\cdot)$ linearized about $\boldsymbol{x}_s$. Assume that the eigenvalues are ordered with respect to decreasing real part; $\mathrm{Re}(\lambda_{i+1}) \leqslant \mathrm{Re}(\lambda_i)$. If all the eigenvalues of (5.3) have negative real parts, the steady state is stable.

Use a Cayley transform to find the eigenvalues γ_i of the system

$$(\boldsymbol{J} - \sigma \boldsymbol{B})^{-1} (\boldsymbol{J} - \mu \boldsymbol{B}) z = \gamma z$$

that are related to the eigenvalues λ_k of (5.3) via

$$\gamma_i = \frac{\lambda_k - \mu}{\lambda_k - \sigma}, \quad i = 1, \ldots, n; k = 1, \ldots, n.$$

Choose $\sigma > 0$ and $\mu = -\sigma$; we choose the value of σ so that it is of similar magnitude to the imaginary part of the eigenvalue of interest, and so that $\sigma > \mathrm{Re}(\lambda_1)$. This transformation has the property of mapping a λ in the right half of the complex plane (i.e. an unstable mode) to a γ outside the unit circle, and those on the left half-plane (i.e. a stable mode) to a γ inside the unit circle. That is,

$$\mathrm{Re}(\lambda) > 0 \Longrightarrow \|\gamma\| > 1.0, \text{ and } \mathrm{Re}(\lambda) < 0 \Longrightarrow \|\gamma\| < 1.0.$$

Since Arnoldi's method will converge more rapidly to those eigenvalues with larger magnitudes, this is a very desirable property for calculating eigenvalues for use in linear stability analysis.

Further details are available in Lehoucq & Salinger (2001), Burroughs *et al.* (2004).

To compute the eigenvalues listed in table 2 we set $g = \beta = \kappa = \nu = 1$ and $f(\theta) = \cos(\theta)$. The mesh has $N/4$ by $N/4$ mesh divisions around a cross-section and $N + N/20$ mesh divisions about the circumference of the loop. For the finest mesh, there are 185 220 unknowns, solved on 64 processors of the Sandia-Intel TFlop machine (ASCI Red) with 333 MHz Pentium processors. The code converges to the steady state easily using a zero initial guess. The number of GMRES solutions required for each eigensolver iteration is approximately 240. The time to compute eigenvalues on the finest mesh is on the order of 2700 s.

6. Conclusions

An examination of flow in a thermosyphon has been conducted using a new PDE model. In the case of a circular loop, the first Fourier modes exactly decouple from all other Fourier modes, leaving a system of three coupled nonlinear PDEs that completely describes the flow in the thermosyphon. This is in contrast to all existing models, which use truncations, adjustable parameters, and other simplifications that are avoided in this formulation.

The use of this model has allowed the identification of stable periodic flows at much lower Prandtl number than predicted by Lorenz-type ODE models. In particular, this model has identified periodic solutions for flows of Prandtl number greater than 18.5.

The trivial solution was found to be globally stable for all Prandtl numbers for $Ra < \gamma_{01}^4$, where γ_{01} is the first zero of the J_0 Bessel function. This global stability limit

https://doi.org/10.1017/S0022112005006361 Published online by Cambridge University Press

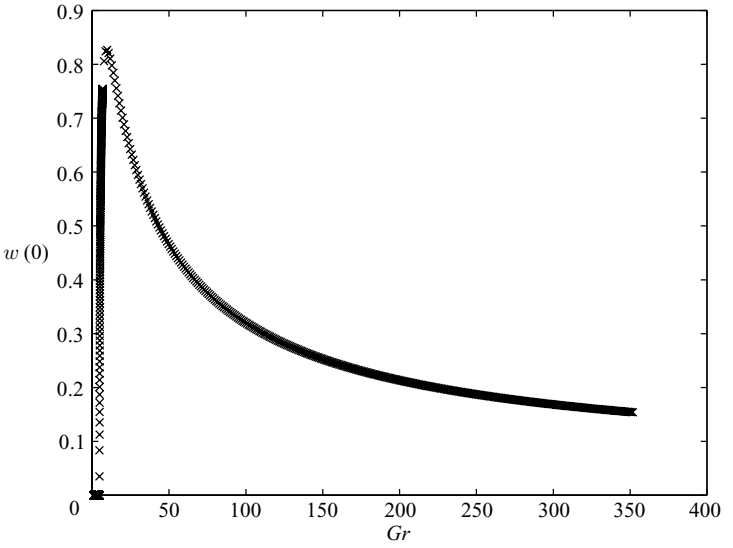


FIGURE 6. The bifurcation diagram at $Pr = 7$.

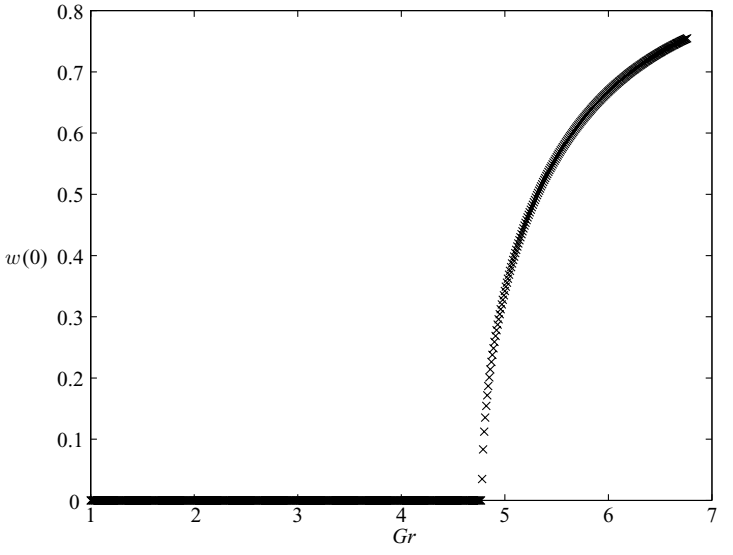


FIGURE 7. An enlargement of the pitchfork bifurcation at $Pr = 7$.

coincides with the location of the first bifurcation, indicating the onset of convection in the thermosyphon.

In figures 6 and 7 the bifurcation diagram is shown for $Pr = 7$. Notice that the thermosyphon runs most efficiently for Grashof number around 10. For values of Grashof greater than 10, the velocity slows. Figures 8–10 show flow profiles calculated with the spectral code. Near the bifurcation point, the velocity profile is not parabolic; rather it has developed a 'dip'. Notice that it is the ϕ component of temperature that drives this change. These profiles show how the Lorenz model will not accurately

https://doi.org/10.1017/S0022112005006361 Published online by Cambridge University Press

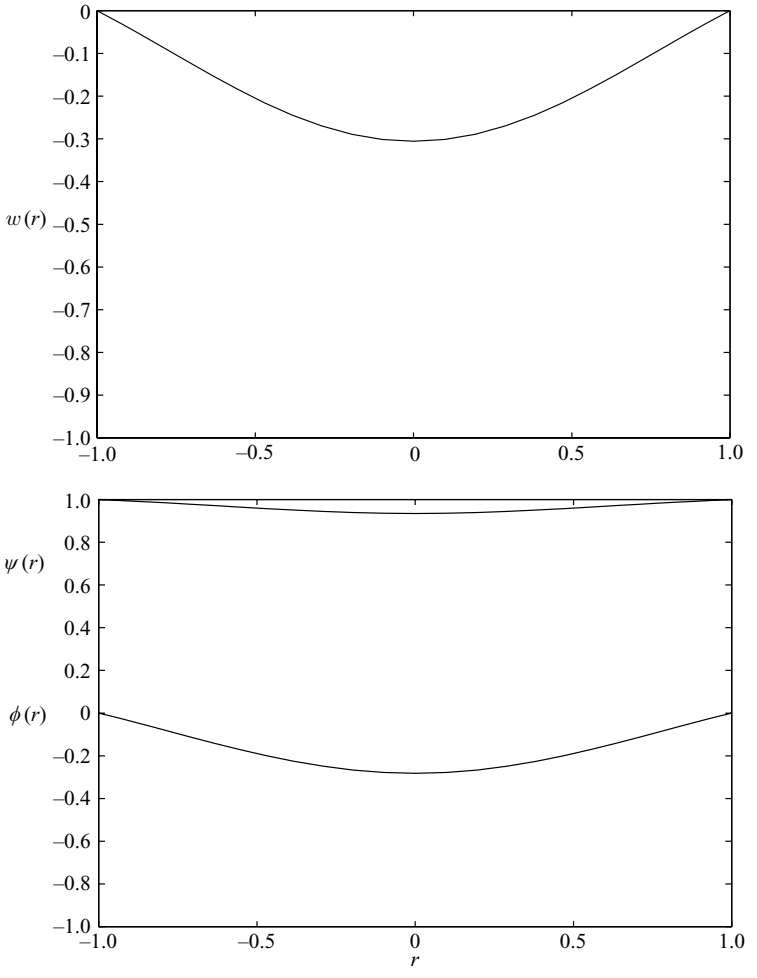


FIGURE 8. Velocity and temperature profiles at $Pr = 7$, $Gr = 5$.

capture the dynamics of the flow in the regions where the profiles are not parabolic. We note that experiments have not been run with sufficiently small aspect ratios to eliminate three-dimensional effects of the flow. For example, experiments by Sano (1991) are run with aspect ratios of approximately 0.03 and 0.01, and by Stern, *et al.* (1988) at 0.05, and both report flows that are not radially symmetric and have three-dimensional effects. It should also be noted that these experiments were run with water and ethyl alcohol, with Prandtl numbers around 7 and 15 respectively, so they do not span the Prandtl numbers in the range of interest of our results, particularly flows with $Pr > 18.5$.

Figure 11 shows the critical Grashof number, Gr_h, as a function of Prandtl number. The Lorenz equations predict that the Hopf bifurcation occurs at the critical value $Gr = 64(Pr + 4)/Pr - 2$; for $Pr = 7$, for example, this gives $Gr = 140.8$, where our analysis shows that the critical value is $Gr = 351.8$; the Lorenz equations underpredict the region where the convective solution is stable. Compare the curves of the predicted Hopf bifurcation by the Lorenz and PDE models in figure 11. Both exhibit a vertical asymptote as a lower bound, but the shape of the curve differs significantly as Pr grows.

https://doi.org/10.1017/S0022112005006361 Published online by Cambridge University Press

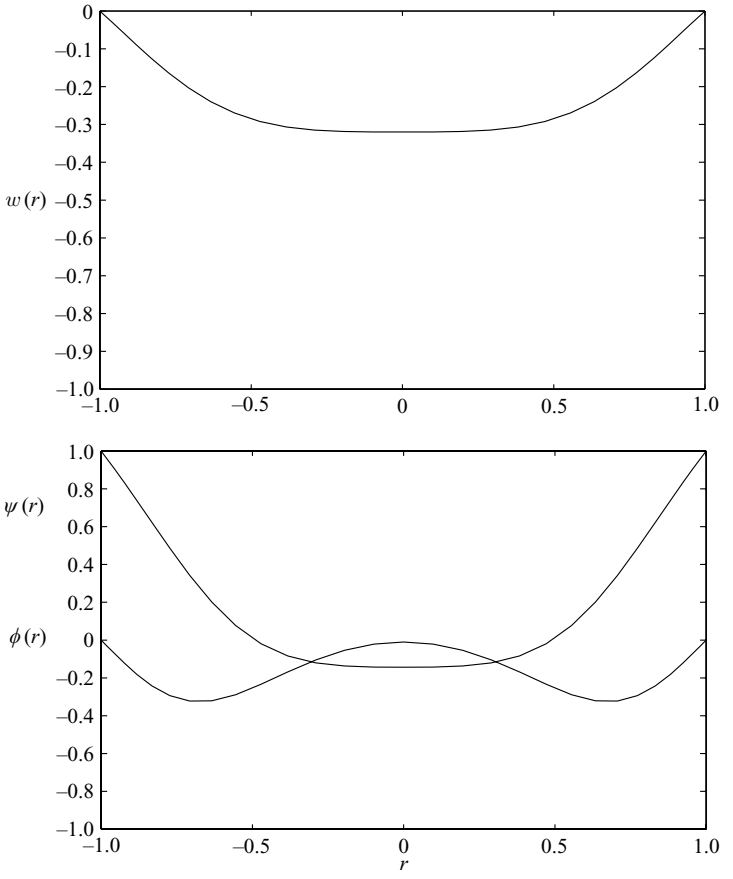


FIGURE 9. Velocity and temperature profiles at $Pr = 7$, $Gr = 100$.

There is significant difference between the Lorenz model and our reduced PDE model in predicting whether the Hopf bifurcation is sub- or supercritical. As discussed in § 4.3, our PDE model predicts that the Hopf bifurcation is subcritical for Prandtl numbers less than 18.5 and supercritical for Prandtl numbers above that value. The Lorenz equations, on the other hand, predict that the Hopf bifurcation is subcritical for this entire range of values. Noting the significant difference in the shape of the curves in figure 11 near $Pr = 18$, it is not surprising that the two models also differ significantly in their predictions of criticality beyond this point.

This material is based upon work supported under a National Science Foundation Graduate Research Fellowship. The authors also gratefully acknowledge the support of Andrew Salinger of Sandia National Laboratories. This work was partially funded by the US Department of Energy through the Accelerated Strategic Computing Initiative and the Mathematical, Information, and Computational Sciences programs.

Sandia is a multiprogram laboratory operated by Sandia Corporation, a Lockheed-Martin Company, for the United States Department of Energy under Contract DE-AC04-94AL85000.

https://doi.org/10.1017/S0022112005006361 Published online by Cambridge University Press

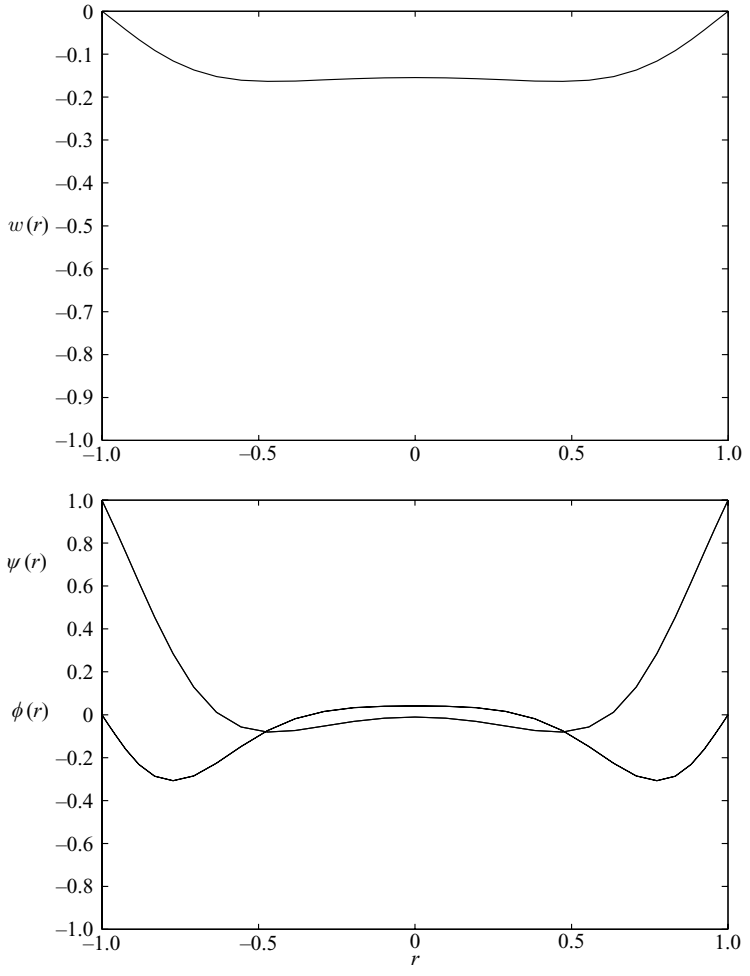


FIGURE 10. Velocity and temperature profiles at $Pr = 7$, $Gr = 350$.

Appendix A. Reduction to the Lorenz model

The Lorenz equations (Lorenz 1963) are a set of ordinary differential equations that, for certain parameter values, provide a simple model of flow in a thermosyphon. Most reported investigations of the thermosyphon problem use a reduction to the Lorenz equations. This type of model exhibits the flow pattern of convection leading to oscillation and chaos. We will compare the simplified PDE model (2.10)–(2.12) to the Lorenz model by imposing a parabolic profile on each of the variables and substituting this into the equations. For simplicity, we will neglect the curvature term on the right-hand side of the ϕ and ψ equations.

It is the assumption of a parabolic profile that leads to the most significant limitations of the Lorenz model. In the flow profiles shown in § 6, one can see that for high values of the Grashof number the profiles deviate dramatically from parabolic. The PDE model proves to be a better model for capturing the nature of the flow in this region.

https://doi.org/10.1017/S0022112005006361 Published online by Cambridge University Press

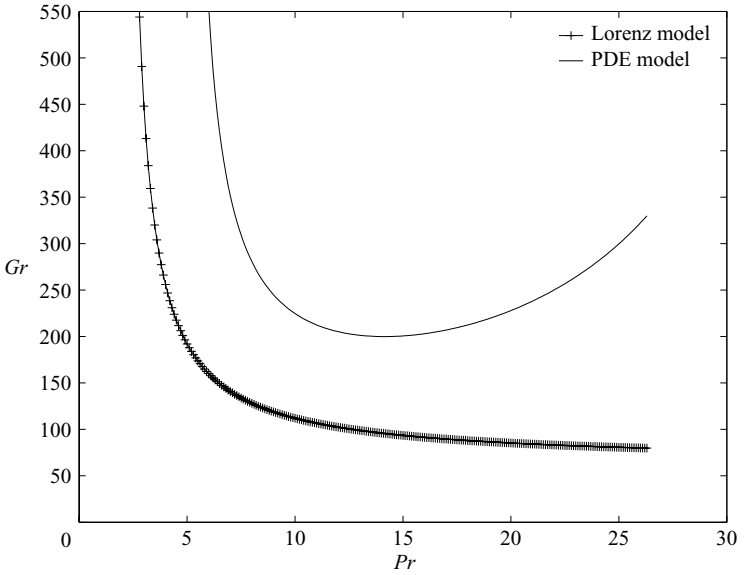


FIGURE 11. The location of the Hopf bifurcation in the Lorenz and PDE models.

To derive the Lorenz model, substitute into (2.10), (2.11), and (2.12)

$$w(r,t) = \hat{w}(t)(r^2-1),$$
$$\phi(r,t) = \hat{\phi}(t)(r^2-1),$$
$$\psi(r,t) = \psi_0 + \hat{\psi}(t)(r^2-1),$$

and integrate over a circle of radius 1 to obtain

$$\frac{\mathrm{d}\hat{w}}{\mathrm{d}t} = -8\hat{w} + Pr\hat{\phi},$$
$$\frac{\mathrm{d}\hat{\phi}}{\mathrm{d}t} = -\frac{8}{Pr}\hat{\phi} - \frac{2Gr}{3Pr}\hat{\psi}\hat{w} + \frac{Gr\psi_0\hat{w}}{Pr},$$
$$\frac{\mathrm{d}\hat{\psi}}{\mathrm{d}t} = -\frac{8}{Pr}\hat{\psi} + \frac{2Gr}{3Pr}\hat{\phi}\hat{w}.$$

Now to correlate these equations to the Lorenz system, introduce

$$\hat{w} = \frac{3\psi_0 P}{16R}X,\ \hat{\phi} = \frac{3\psi_0}{2R}Y,\ \hat{\psi} = \frac{3\psi_0}{2R}Z,\ t = \frac{P}{8}T,\ Pr = P,\ Gr = \frac{64R}{\psi_0 P} \qquad \text{(A 1)}$$

to arrive at the set of equations

$$\frac{\mathrm{d}X}{\mathrm{d}T} = -PX + PY,$$
$$\frac{\mathrm{d}Y}{\mathrm{d}T} = -Y + RX - XZ,$$
$$\frac{\mathrm{d}Z}{\mathrm{d}T} = -Z + XY.$$

which correspond to the Lorenz system (see Tritton 1988).

https://doi.org/10.1017/S0022112005006361 Published online by Cambridge University Press

Appendix B. Global stability of the trivial branch

We will analyse the global stability of the trivial solution. There is a limit of the parameters (Grashof number and Prandtl number) below which any perturbation will settle to the trivial solution. This limit is identical to the pitchfork bifurcation point found in § 3. Because we will show that the trivial branch is globally stable up to the pitchfork bifurcation point, this provides a proof that the pitchfork bifurcation is supercritical.

The proof of global stability will proceed as follows. First we will define an energy function that depends on a parameter λ. The rate of change of energy can be maximized by a function $Gr(\lambda)$ of the Grashof number, and each value of λ corresponds to a different energy rate. We will show that this rate of change of energy is always negative. Then maximizing this function of Grashof number over all values of λ, we find the optimal energy function, that is, the one that gives the largest value of Gr for which a decaying energy rate can be guaranteed. This value of Gr is the global stability limit, and corresponds to the pitchfork bifurcation point.

To facilitate the analysis, rescale equations (2.10)–(2.12) so that the Grashof number appears symmetrically. Define

$$w = \sqrt{Gr}\tilde{w}.$$

Then equations (B 1)–(B 3) become

$$Pr\phi_t = \sqrt{Gr}\tilde{w}\psi + \nabla^2\phi, \tag{B 1}$$

$$Pr\psi_t = -\sqrt{Gr}\tilde{w}\phi + \nabla^2\psi, \tag{B 2}$$

$$\tilde{w}_t = \sqrt{Gr}Pr\phi + \nabla^2\tilde{w}, \tag{B 3}$$

along with boundary conditions

$$\phi(1) = w(1) = 0,$$
$$\psi(1) = 1.$$

For simplicity, we will drop the tilde on the w.

Consider a disturbance $(\hat{\phi}, \hat{\psi}, \hat{w})$ about the base flow (ϕ_0, ψ_0, w_0); for the trivial branch, this base flow is $(0, 1, 0)$, so that

$$(\phi, \psi, w) = (0 + \hat{\phi}, 1 + \hat{\psi}, 0 + \hat{w}).$$

The disturbance to the base flow satisfies:

$$\hat{\phi}_t = \frac{\sqrt{Gr}}{Pr}\hat{w} + \frac{\sqrt{Gr}}{Pr}\hat{w}\hat{\psi} + \frac{1}{Pr}\nabla^2\hat{\phi},$$

$$\hat{\psi}_t = -\frac{\sqrt{Gr}}{Pr}\hat{w}\hat{\phi} + \frac{1}{Pr}\nabla^2\hat{\psi},$$

$$\hat{w}_t = \sqrt{Gr}Pr\hat{\phi} + \nabla^2\hat{w}.$$

From here on we drop the hat notation.

Now form a family of energy functions that depend on the parameter λ:

$$E = \langle\phi^2\rangle + \langle\psi^2\rangle + \lambda\langle w^2\rangle, \tag{B 4}$$

where $\langle u, v\rangle$ denotes the integral $\int_0^1 u(r)^T v(r) r \, \mathrm{d}r$:

$$\langle\phi_t, \phi\rangle + \langle\psi_t, \psi\rangle + \lambda\langle w_t, w\rangle$$
$$= \frac{\sqrt{Gr}}{Pr}\langle w, \phi\rangle + \lambda\sqrt{Gr}Pr\langle\phi, w\rangle + \frac{1}{Pr}\langle\nabla^2\phi, \phi\rangle + \frac{1}{Pr}\langle\nabla^2\psi, \psi\rangle + \lambda\langle\nabla^2 w, w\rangle.$$

https://doi.org/10.1017/S0022112005006361 Published online by Cambridge University Press

Use Green's identity to rewrite the Laplacian terms, using that the disturbance satisfies null boundary conditions, and Reynolds Transport Theorem to rewrite the time derivative terms. This leads to the following theorem:

THEOREM B.1. *For equations (B 1)–(B 3), the energy defined by the family of curves (B 4) satisfies the following equation:*

$$\frac{\partial E}{\partial t} = \frac{\sqrt{Gr}}{Pr}(1 + \lambda Pr^2)\langle w, \phi\rangle - \frac{1}{Pr}\langle|\nabla\phi|^2\rangle - \frac{1}{Pr}\langle|\nabla\psi|^2\rangle - \lambda\langle|\nabla w|^2\rangle. \tag{B 5}$$

This equation is made up of the energy dissipation terms (the gradient terms) and the energy production terms. We wish to find the balance between dissipation and production terms so that the total rate of change of energy will always be negative, keeping in mind that this equation defines the energy for a family of curves, one for each λ.

First we will show that for each λ there is a maximum Grashof number where this rate of change of energy is always negative. Then we will maximize this over all λ to find the optimal energy function.

Equation (B 5) is of the form

$$\frac{\partial E}{\partial t} = \int_0^1 F(r, \boldsymbol{y}, \boldsymbol{y}')r \, \mathrm{d}r := J$$

where $\boldsymbol{y} = (\phi, \psi, w)^T$. Notice that J is a quadratic functional; it is because of this that the following analysis holds.

It is clear that for $Gr = 0$, $\partial E/\partial t$ is negative, and that for small values of Gr, there is still decay. There is a critical value of Gr where there will cease to be decay; one can employ the Calculus of Variations to calculate this critical value.

First we will formulate the problem as a minimization problem. The critical Gr is bounded above if the ratio of the dissipation to production is bounded below. That is,

$$\sqrt{Gr} < \min\left(\frac{-\frac{1}{Pr}\langle|\nabla\phi|^2\rangle - \frac{1}{Pr}\langle|\nabla\psi|^2\rangle - \lambda\langle|\nabla w|^2\rangle}{\frac{1}{Pr}(1 + \lambda Pr^2)\langle w, \phi\rangle}\right).$$

The 'decay constant lemma' proved by Joseph (1976) guarantees the existence of a lower bound for this ratio.

One can use the Calculus of Variations to solve this minimization problem, and this yields an eigenvalue problem. Taking the first variation of J, one gets

$$\delta J = \int_0^1 \left(F_y - \frac{\mathrm{d}}{\mathrm{d}r}F_{y'}\right)h(r)r \, \mathrm{d}r = 0.$$

The solutions $\boldsymbol{y}$ satisfy null boundary conditions. Using the Fundamental Lemma of the Calculus of Variations, the Euler–Lagrange equation must be satisfied:

$$F_y - \frac{\mathrm{d}}{\mathrm{d}r}F_{y'} = 0,$$

which is the eigenvalue problem

$$\sqrt{Gr}\left(\frac{1 + \lambda Pr^2}{Pr}\right)w + \frac{2}{Pr}\nabla^2\phi = 0,$$

https://doi.org/10.1017/S0022112005006361 Published online by Cambridge University Press

$$\frac{2}{Pr}\nabla^2\psi = 0,$$
$$\sqrt{Gr}\left(\frac{1+\lambda Pr^2}{Pr}\right)\phi + 2\lambda\nabla^2 w = 0.$$

The equation for ψ decouples and is independent of Gr. Now notice that this is of the same form as the eigenvalue problem solved in the linear stability analysis of the pitchfork bifurcation, equation (3.1). The solutions of this eigenvalue problem have the form

$$\begin{pmatrix}\phi\\ w\end{pmatrix} = \begin{pmatrix}c_1\\ c_2\end{pmatrix} J_0(\gamma_{m0}r)$$

where $\gamma = \gamma_{0,k}$, $k = 1, 2, 3, \ldots$, is a zero of the J_0 Bessel function. From $\nabla^2\phi = -\gamma_{0k}^2\phi$ and $\nabla^2 w = -\gamma_{0k}^2 w$ obtain the condition

$$\begin{vmatrix} \dfrac{-\gamma_{0k}^2}{Pr} & \dfrac{\sqrt{Gr}}{2Pr}(1+\lambda Pr^2) \\ \left(\dfrac{\sqrt{Gr}}{2Pr}\right)(1+\lambda Pr^2) & -\lambda\gamma_{0k}^2 \end{vmatrix} = 0.$$

The result is stated as a theorem.

THEOREM B.2. *The critical Gr is given by the following equation:*

$$Gr(\lambda) = \frac{4\lambda\gamma_{0k}^4 Pr}{(1+\lambda Pr^2)^2}.$$

Each value of λ corresponds to a Grashof number that is the maximum value for which the energy will always decay. Take the derivative with respect to λ to find the value of λ that maximizes Gr. This is easily seen to be $\lambda = 1/Pr^2$, leading to

$$Gr \leqslant \frac{\gamma_{0k}^4}{Pr}.$$

Depending on the specific root $\gamma_{0,k}$ of J_0, the decay rate has a negative extremum at $Gr = \gamma_{0k}^4/Pr$. However, only the value $k = 1$ corresponds to a maximum, as is shown below.

B.1. *Details of the maximization*

The first variation has only determined that there is an extremum; it must be shown that there is a maximum. Use the following theorem (Gelfand & Fomin 1991):

THEOREM B.3. *If $P(x) > 0$ and $[a, b]$ contains no conjugate points to a, then $\int_a^b (Ph'^2 + Qh^2)\mathrm{d}x$ is positive definite for all $h(x)$ such that $h(a) = h(b) = 0$.*

A conjugate point $\tilde{a}$ to a is defined as a point for which $-(\mathrm{d}/\mathrm{d}x)Ph' + Qh = 0$ has a solution that vanishes for $x = a$ and $x = \tilde{a}$ but is not identically 0.

The original formulation is of the form

$$\int_0^1 (P\,\mathbf{y}'^2 + Q\,\mathbf{y}^2)r\ \mathrm{d}r,$$

where $P(x)$ is

$$\mathrm{diag}\left[\frac{-1}{Pr}, \frac{-1}{Pr}, -\lambda\right].$$

https://doi.org/10.1017/S0022112005006361 Published online by Cambridge University Press

For the region to contain no conjugate points, choose the first Bessel zero, $\gamma = \gamma_{01}$, and then the rate of change of energy, $\partial E/\partial t$, is negative definite, so the extremum found is a maximum.

The global stability limit for the trivial solution is identical to the linear stability limit for this non-convective branch, which in terms of Ra is

$$Ra_p = \gamma_{01}^4.$$

Appendix C. Hopf analysis

We analyse the convective solution to the system (2.15) and (2.16). Making the substitutions $s = \omega t$ and $\tau = \epsilon^2 s$, write the system as follows:

$$(\omega \boldsymbol{D}\partial_s + \epsilon^2 \boldsymbol{D}\partial_\tau - \boldsymbol{I}\nabla^2 - \boldsymbol{P})\boldsymbol{u} = Gr\boldsymbol{F}(\boldsymbol{u}).$$

Expand the solution

$$\boldsymbol{u} = \boldsymbol{u}_0(r) + \epsilon \boldsymbol{u}_1(s, \tau, r) + \epsilon^2 \boldsymbol{u}_2(s, \tau, r) + \epsilon^3 \boldsymbol{u}_3(s, \tau, r) + O(\epsilon^4).$$

Expand the Grashof number as

$$Gr = Gr_h + j\epsilon^2,$$

where $j = \pm 1$, with $j = +1$ corresponding to $Gr > Gr_h$ and $j = -1$ corresponding to $Gr < Gr_h$. Expand the frequency as

$$\omega = \omega_0 + \epsilon\omega_1 + \epsilon^2\omega_2.$$

This leads to the system

$$\begin{aligned}&((\omega_0 D\partial_s - I\nabla^2 - P) + \epsilon\omega_1 D\partial_s + \epsilon^2(\omega_2 D\partial_s + D\partial_\tau)) \sum_{k=1}^{n} \epsilon^k \boldsymbol{u}_k \\ &= \left(u_{30} M \boldsymbol{u}_0 + \sum_{k=1}^{n} \epsilon^k \left(\sum_{l=1}^{k-1} u_{3k-l} M \boldsymbol{u}_l \right) + \sum_{k=1}^{n} \epsilon^k J_0 \boldsymbol{u}_k \right) (Gr_h + j\epsilon^2)\end{aligned}$$

where u_{ij} denotes the ith component of $\boldsymbol{u}_j$ and J_0 is the zero-order Bessel function. The operators at each order are

$$\begin{aligned}\boldsymbol{L}_0 &= \omega_0 \boldsymbol{D}\partial_s - \boldsymbol{I}\nabla^2 - \boldsymbol{P}, \\ \boldsymbol{L}_1 &= \omega_1 \boldsymbol{D}\partial_s, \\ \boldsymbol{L}_2 &= \omega_2 \boldsymbol{D}\partial_s + \boldsymbol{D}\partial_\tau, \\ \boldsymbol{L}_3 &= \omega_3 \boldsymbol{D}\partial_s + \omega_1 \boldsymbol{D}\partial_\tau.\end{aligned}$$

The systems at each order are:

O(ϵ^0):

$$\boldsymbol{L}_0 \boldsymbol{u}_0 = Gr_h u_{30} \boldsymbol{M}\boldsymbol{u}_0.$$

O(ϵ):

$$(\boldsymbol{L}_0 - Gr_h \boldsymbol{J}_0)\boldsymbol{u}_1 = -\boldsymbol{L}_1 \boldsymbol{u}_0.$$

O(ϵ^2):

$$(\boldsymbol{L}_0 - Gr_h \boldsymbol{J}_0)\boldsymbol{u}_2 = -\boldsymbol{L}_1 \boldsymbol{u}_1 - \boldsymbol{L}_2 \boldsymbol{u}_0 + Gr_h u_{31} \boldsymbol{M}\boldsymbol{u}_1 + j u_{30} \boldsymbol{M}\boldsymbol{u}_0.$$

O(ϵ^3):

$$(\boldsymbol{L}_0 - Gr_h \boldsymbol{J}_0)\boldsymbol{u}_3 = -\boldsymbol{L}_3 \boldsymbol{u}_0 - \boldsymbol{L}_1 \boldsymbol{u}_2 - \boldsymbol{L}_2 \boldsymbol{u}_1 + Gr_h u_{32} \boldsymbol{M}\boldsymbol{u}_1 + Gr_h u_{31} \boldsymbol{M}\boldsymbol{u}_2 + j \boldsymbol{J}_0 \boldsymbol{u}_1.$$

https://doi.org/10.1017/S0022112005006361 Published online by Cambridge University Press

We now outline the steps in the asymptotic analysis. Compute $\boldsymbol{u}_0$ by solving the steady-state equations to get a solution $\boldsymbol{u}_0(r)$. Because $\boldsymbol{u}_0$ is independent of time, $\boldsymbol{L}_1\boldsymbol{u}_0 = \boldsymbol{L}_2\boldsymbol{u}_0 = \boldsymbol{L}_3\boldsymbol{u}_0 = 0$.

At order ϵ,

$$(\boldsymbol{L}_0 - Gr_h\boldsymbol{J}_0)\boldsymbol{u}_1 = 0.$$

Compute $\boldsymbol{u}_1$ by solving the eigenvalue problem to obtain

$$\boldsymbol{u}_1 = a(\tau)\boldsymbol{A}(r)\mathrm{e}^{\mathrm{i}s} + \bar{a}(\tau)\bar{\boldsymbol{A}}(r)\mathrm{e}^{-\mathrm{i}s},$$

where the bar notation denotes the complex conjugate, and ω_0.

At order ϵ^2,

$$(\boldsymbol{L}_0 - Gr_h\boldsymbol{J}_0)\boldsymbol{u}_2 = -\boldsymbol{L}_1\boldsymbol{u}_1 + Gr_h u_{31}\boldsymbol{M}\boldsymbol{u}_1 + ju_{30}\boldsymbol{M}\boldsymbol{u}_0.$$

The term $\boldsymbol{L}_1\boldsymbol{u}_1$ will produce expressions in $\mathrm{e}^{\mathrm{i}s}$, which are resonant terms. Then to suppress these resonant terms choose $\omega_1 = 0$. The other terms on the right-hand side will produce expressions in $\mathrm{e}^0, \mathrm{e}^{2\mathrm{i}s}$, and $\mathrm{e}^{-2\mathrm{i}s}$, so compute the solution $\boldsymbol{u}_2$ using the method of undetermined coefficients, by solving a system $Lu = b$ for each of the harmonic terms.

Formulate the $O(\epsilon^3)$ problem and use Fredholm's Alternative Theorem (Keener 1995) to find a solvability condition.

C.1. *Second-order problem*

At order ϵ^2, the right-hand side is

$$ju_{30}\boldsymbol{M}\boldsymbol{u}_0 + Gr_h u_{31}\boldsymbol{M}\boldsymbol{u}_1.$$

Examine each term. First,

$$ju_{30}\boldsymbol{M}\boldsymbol{u}_0 = j\begin{pmatrix} u_{30}u_{20} \\ -u_{30}u_{10} \\ 0 \end{pmatrix}$$

which is known from the order-ϵ^0 equation. Second, using the notation A_{ij} for the ith component of $\boldsymbol{A}_j$,

$$\begin{aligned} Gr_h u_{31}\boldsymbol{M}\boldsymbol{u}_1 &= Gr_h(aA_{31}\mathrm{e}^{\mathrm{i}s} + \bar{a}\bar{A}_{31}\mathrm{e}^{-\mathrm{i}s})\boldsymbol{M}(a\boldsymbol{A}_1\mathrm{e}^{\mathrm{i}s} + \bar{a}\bar{\boldsymbol{A}}_1\mathrm{e}^{-\mathrm{i}s}) \\ &= 2a\bar{a}Gr_h\begin{pmatrix} A_{31}\bar{A}_{21} \\ -A_{31}\bar{A}_{11} \\ 0 \end{pmatrix} + a^2Gr_h\begin{pmatrix} A_{31}A_{21} \\ -A_{31}A_{11} \\ 0 \end{pmatrix}\mathrm{e}^{2\mathrm{i}s} + \bar{a}^2Gr_h\begin{pmatrix} \bar{A}_{31}\bar{A}_{21} \\ -\bar{A}_{31}\bar{A}_{11} \\ 0 \end{pmatrix}\mathrm{e}^{-2\mathrm{i}s}, \end{aligned}$$

so the right-hand side is

$$\begin{aligned} &j\begin{pmatrix} u_{30}u_{20} \\ -u_{30}u_{10} \\ 0 \end{pmatrix} + 2|a|^2Gr_h\mathrm{Re}\left(\begin{pmatrix} A_{31}\bar{A}_{21} \\ -A_{31}\bar{A}_{11} \\ 0 \end{pmatrix}\right) \\ &+a^2Gr_h\begin{pmatrix} A_{31}A_{21} \\ -A_{31}A_{11} \\ 0 \end{pmatrix}\mathrm{e}^{2\mathrm{i}s} + \bar{a}^2Gr_h\begin{pmatrix} \bar{A}_{31}\bar{A}_{21} \\ -\bar{A}_{31}\bar{A}_{11} \\ 0 \end{pmatrix}\mathrm{e}^{-2\mathrm{i}s}. \end{aligned}$$

https://doi.org/10.1017/S0022112005006361 Published online by Cambridge University Press

Solving with this right-hand side leads to a solution

$$\boldsymbol{u}_2 = \begin{pmatrix} u_{12} \\ u_{22} \\ u_{32} \end{pmatrix} := \boldsymbol{B}_0(r) + (a^2 \boldsymbol{B}_2(r) \mathrm{e}^{2\mathrm{i}s} + \text{c.c. }),$$

where

$$\boldsymbol{B}_0 = j\boldsymbol{b}_0^{(1)}(r) + |a|^2 \boldsymbol{b}_0^{(2)}(r)$$

is the solution of a real PDE with a real right-hand side, and so is real. Note that the vectors $\boldsymbol{B}_0$ and $\boldsymbol{B}_2$ are computed numerically.

C.2. *The Landau equation*

Apply Fredholm's Alternative Theorem (Keener 1995) at order ϵ^3, adopting the notation used in Joseph (1976)

$$\langle \boldsymbol{a} \cdot \bar{\boldsymbol{b}} \rangle = \int_0^1 \boldsymbol{a} \cdot \bar{\boldsymbol{b}} r \, \mathrm{d}r$$

$$[\boldsymbol{a}, \boldsymbol{b}] = \frac{1}{T} \int_0^T \langle \boldsymbol{a} \cdot \bar{\boldsymbol{b}} \rangle \, \mathrm{d}t.$$

Solve the adjoint homogeneous problem,

$$(\boldsymbol{L}_0 - Gr_h \boldsymbol{J}_0)^* z = 0$$

and then require for solvability that $\boldsymbol{f}$, the right-hand side at order ϵ^3, satisfies

$$[\boldsymbol{f}, z] = 0.$$

The order-ϵ^3 right-hand side is

$$-\boldsymbol{L}_2 \boldsymbol{u}_1 + Gr_h u_{32} \boldsymbol{M} \boldsymbol{u}_1 + Gr_h u_{31} \boldsymbol{M} \boldsymbol{u}_2 + j\boldsymbol{J}_0 \boldsymbol{u}_1.$$

Examine each term. First,

$$\begin{aligned} -\boldsymbol{L}_2 \boldsymbol{u}_1 &= -(\omega_2 \boldsymbol{D} \partial_s + \boldsymbol{D} \partial_\tau)[a\boldsymbol{A}_1 \mathrm{e}^{\mathrm{i}s} + \bar{a}\bar{\boldsymbol{A}}_1 \mathrm{e}^{-\mathrm{i}s}] \\ &= -\omega_2 \boldsymbol{D}[a\mathrm{i}\boldsymbol{A}_1 \mathrm{e}^{\mathrm{i}s} - \bar{a}\mathrm{i}\bar{\boldsymbol{A}}_1 \mathrm{e}^{-\mathrm{i}s}] - \left[\frac{\mathrm{d}a}{\mathrm{d}\tau} D\boldsymbol{A}_1 \mathrm{e}^{\mathrm{i}s} + \frac{\mathrm{d}\bar{a}}{\mathrm{d}\tau} D\bar{\boldsymbol{A}}_1 \mathrm{e}^{-\mathrm{i}s} \right]. \end{aligned}$$

Second, using the notation B_{ij} for the ith component of $\boldsymbol{B}_j$ and $b_{ij}^{(k)}$ for the ith component of $\boldsymbol{b}_j^{(k)}$,

$$\begin{aligned} Gr_h u_{32} \boldsymbol{M} \boldsymbol{u}_1 &= Gr_h (B_{30} + a^2 B_{32} \mathrm{e}^{2\mathrm{i}s} + \bar{a}^2 \bar{B}_{32} \mathrm{e}^{-2\mathrm{i}s}) \boldsymbol{M} (a\boldsymbol{A}_1 \mathrm{e}^{\mathrm{i}s} + \bar{a}\bar{\boldsymbol{A}}_1 \mathrm{e}^{-\mathrm{i}s}) \\ &= Gr_h \begin{pmatrix} jb_{30}^{(1)}(aA_{21}\mathrm{e}^{\mathrm{i}s}) + b_{30}^{(2)}(a^2\bar{a}A_{21}\mathrm{e}^{\mathrm{i}s}) + (a^2\bar{a}B_{32}\bar{A}_{21}\mathrm{e}^{\mathrm{i}s}) \\ -j\left(b_{30}^{(1)}(aA_{11}\mathrm{e}^{\mathrm{i}s}) + b_{30}^{(2)}(a^2\bar{a}A_{11}\mathrm{e}^{\mathrm{i}s}) + (a^2\bar{a}B_{32}\bar{A}_{11}\mathrm{e}^{\mathrm{i}s})\right) \\ 0 \end{pmatrix} + \text{c.c.} \end{aligned}$$

Third,

$$\begin{aligned} Gr_h u_{31} \boldsymbol{M} \boldsymbol{u}_2 &= Gr_h (a A_{31} \mathrm{e}^{\mathrm{i}s}) \boldsymbol{M} \left(j\boldsymbol{b}_0^{(1)} + |a|^2 \boldsymbol{b}_0^{(2)} + a^2 \boldsymbol{B}_2 \mathrm{e}^{2\mathrm{i}s} \right) \\ &= Gr_h \begin{pmatrix} jb_{20}^{(1)}(aA_{31}\mathrm{e}^{\mathrm{i}s}) + b_{20}^{(2)}(a^2\bar{a}A_{31}\mathrm{e}^{\mathrm{i}s}) + j(a^2\bar{a}B_{22}\bar{A}_{31}\mathrm{e}^{\mathrm{i}s}) \\ b_{10}^{(1)}(aA_{31}\mathrm{e}^{\mathrm{i}s}) + b_{10}^{(2)}(a^2\bar{a}A_{31}\mathrm{e}^{\mathrm{i}s}) + (a^2\bar{a}B_{12}\bar{A}_{31}\mathrm{e}^{\mathrm{i}s}) \\ 0 \end{pmatrix} + \text{c.c.} \end{aligned}$$

https://doi.org/10.1017/S0022112005006361 Published online by Cambridge University Press

Lastly,

$$j\boldsymbol{J}_0\boldsymbol{u}_1 = ja\begin{pmatrix} u_{30}A_{21}+u_{20}A_{31} \\ -u_{30}A_{11}-u_{10}A_{31} \\ 0 \end{pmatrix}\mathrm{e}^{\mathrm{i}s}+\text{c.c.}$$

Therefore, the right-hand side is

$$\begin{aligned}
&-\omega_2\boldsymbol{D}[a\mathrm{i}\boldsymbol{A}_1\mathrm{e}^{\mathrm{i}s}+\text{c.c. }]-\left[\frac{\mathrm{d}a}{\mathrm{d}\tau}\boldsymbol{D}\boldsymbol{A}_1\mathrm{e}^{\mathrm{i}s}+\text{c.c.}\right] \\
&+Gr_h\begin{pmatrix} jb_{30}^{(1)}(aA_{21}\mathrm{e}^{\mathrm{i}s})+jb_{30}^{(2)}(a^2\bar{a}A_{21}\mathrm{e}^{\mathrm{i}s})+(a^2\bar{a}B_{32}\bar{A}_{21}\mathrm{e}^{\mathrm{i}s}) \\ -\big(b_{30}^{(1)}(aA_{11}\mathrm{e}^{\mathrm{i}s})+b_{30}^{(2)}(a^2\bar{a}A_{11}\mathrm{e}^{\mathrm{i}s})+(a^2\bar{a}B_{32}\bar{A}_{11}\mathrm{e}^{\mathrm{i}s})\big) \\ 0 \end{pmatrix}+\text{c.c.} \\
&+Gr_h\begin{pmatrix} jb_{20}^{(1)}(aA_{31}\mathrm{e}^{\mathrm{i}s})+jb_{20}^{(2)}(a^2\bar{a}A_{31}\mathrm{e}^{\mathrm{i}s})+(a^2\bar{a}B_{22}\bar{A}_{31}\mathrm{e}^{\mathrm{i}s}) \\ b_{10}^{(1)}(aA_{31}\mathrm{e}^{\mathrm{i}s})+b_{10}^{(2)}(a^2\bar{a}A_{31}\mathrm{e}^{\mathrm{i}s})+(a^2\bar{a}B_{12}\bar{A}_{31}\mathrm{e}^{\mathrm{i}s}) \\ 0 \end{pmatrix}+\text{c.c.} \\
&+ja\begin{pmatrix} u_{30}A_{21}+u_{20}A_{31} \\ -u_{30}A_{11}-u_{10}A_{31} \\ 0 \end{pmatrix}\mathrm{e}^{\mathrm{i}s}+\text{c.c.}
\end{aligned}$$

Now enforce

$$[\boldsymbol{f},\boldsymbol{z}]=0.$$

Compute the time integral of this solvability condition first; then the only non-zero components are constant in time (s). These terms are

$$\begin{aligned}
&-\omega_2\boldsymbol{D}a\mathrm{i}\boldsymbol{A}_1\cdot\bar{\boldsymbol{z}}-\frac{\mathrm{d}a}{\mathrm{d}\tau}\boldsymbol{D}\boldsymbol{A}_1\cdot\bar{\boldsymbol{z}}+jGr_ha\begin{pmatrix} b_{30}^{(1)}A_{21} \\ b_{30}^{(1)}A_{11} \\ 0 \end{pmatrix}\cdot\bar{\boldsymbol{z}}+jGr_ha\begin{pmatrix} b_{20}^{(1)}A_{31} \\ b_{10}^{(1)}A_{31} \\ 0 \end{pmatrix}\cdot\bar{\boldsymbol{z}} \\
&+ja\begin{pmatrix} u_{30}A_{21}+u_{20}A_{31} \\ -u_{30}A_{11}-u_{10}A_{31} \\ 0 \end{pmatrix}\bar{\boldsymbol{z}}+Gr_ha^2\bar{a}\begin{pmatrix} b_{30}^{(2)}A_{21} \\ b_{30}^{(2)}A_{11} \\ 0 \end{pmatrix}\cdot\bar{\boldsymbol{z}} \\
&+Gr_ha^2\bar{a}\begin{pmatrix} b_{20}^{(2)}A_{31} \\ b_{10}^{(2)}A_{31} \\ 0 \end{pmatrix}\cdot\bar{\boldsymbol{z}}+Gr_ha^2\bar{a}\begin{pmatrix} B_{32}\bar{A}_{21}+B_{22}\bar{A}_{31} \\ B_{32}\bar{A}_{11}+B_{12}\bar{A}_{31} \\ 0 \end{pmatrix}\cdot\bar{\boldsymbol{z}}.
\end{aligned}$$

Now compute the volume integral of these terms and set it to zero, arriving at an ODE in a:

$$\alpha_0\frac{\mathrm{d}a}{\mathrm{d}\tau}=j\alpha a+\beta a|a|^2 \tag{C 1}$$

where the coefficients α_0, α and β are determined via the volume integral.

The nature of the bifurcation has been reduced to the study of an ODE. Use the Hopf bifurcation theorem as stated in Glendinning (1994):

https://doi.org/10.1017/S0022112005006361 Published online by Cambridge University Press

THEOREM C.1. *Hopf Bifurcation Theorem, Subcritical Case*

Suppose that $\dot{x} = f(x, y, \mu)$, $\dot{y} = g(x, y, \mu)$ *with* $f(0, 0, \mu) = g(0, 0, \mu) = 0$ *and that the Jacobian matrix evaluated at the origin when* $\mu = 0$ *is*

$$\begin{pmatrix} 0 & -\omega \\ \omega & 0 \end{pmatrix}$$

for some $\omega \neq 0$. *If* $f_{\mu x} + g_{\mu y} \neq 0$ *and* $c \neq 0$ *then a curve of periodic solutions bifurcates from the origin into* $\mu < 0$ *if* $c(f_{mux} + g_{\mu y}) > 0$. *If* $f_{\mu x} + g_{\mu y} > 0$, *then the origin is stable for* $\mu < 0$ *and unstable for* $\mu > 0$. *If the origin is stable on the side of* $\mu = 0$ *for which the periodic solutions exist, the periodic solutions are unstable and the bifurcation is subcritical. The constant c is given by*

$$c = \frac{1}{16}(f_{xxx} + g_{xxy} + f_{xyy} + g_{yyy}) + \frac{1}{16\omega}(f_{xy}(f_{xx} + f_{yy}) - g_{xy}(g_{xx} + g_{yy}) - f_{xx}g_{xx} + f_{yy}g_{yy})$$

evaluated at $(x, y) = (0, 0)$.

This theorem can be applied as follows. Rescale the equation (C 1) to get

$$\frac{\mathrm{d}a}{\mathrm{d}\tau} = j\alpha a + \beta|a|^2 a.$$

Then breaking the system into its real and imaginary parts, it is in the form in the theorem as stated above. The requirements for a subcritical bifurcation are met when $j = -1$ and $\alpha_r < 0, \beta_r > 0$. The computation of these coefficients is straightforward and is being undertaken at this time.

REFERENCES

ASCHER, U. M., RUUTH, S. J. & WETTON, B. T. R. 1995 Implicit-explicit methods for time-dependent partial differential equations. *SIAM J. Numer. Anal.* **32**, 797–823.

BERGERON, K., COUTSIAS, E. A., LYNOV, J. P. & NIELSEN, A. H. 2000 Dynamical properties of forced shear layers in an annular geometry. *J. Fluid Mech.* **402**, 255–289.

BOSKOVIC, D. & KRSTIC, M. 2001 Nonlinear stabilization of a thermal convection loop by state feedback. *Automatica* **37**, 2033–2040.

BURROUGHS, E. A., ROMERO, L. A., LEHOUCQ, R. B. & SALINGER, A. G. 2001 Large scale eigenvalue calculations for computing the stability of buoyancy driven flows. *Tech. Rep.* SAND2001–0113, Sandia National Laboratories, Albuquerque, NM.

BURROUGHS, E., ROMERO, L., LEHOUCQ, R. & SALINGER, A. 2004 Linear stability of flow in a differentially heated cavity via large-scale eigenvalue calculations. *Intl J. Numer. Meth. Heat Fluid Flow* **14**, 803–822.

BUSSE, F. H. & CLEVER, R. M. 1979 Instabilities of convection rolls of moderate Prandtl number. *Journal of Fluid Mechanics* **91**, 319–335.

CANUTO, C., HUSSAINI, M., QUARTERONI, A. & ZANG, T. 1988 *Spectral Methods in Fluid Dynamics.* Springer.

CHANDRASEKHAR, S. 1961 *Hydrodynamic and Hydromagnetic Stability*. Dover.

COUTSIAS, E. A., HAGSTROM, T., HESTHAVEN, J. & TORRES, D. C. 1995 Integration preconditioners for differential operators in spectral tau-methods. In *ICOSAHOM-95. Proc. 3. Intl Conf. on Spectral and High Order Methods* (ed. L. Ilin & A. V. Ridg-way Scott), pp. 21–38. Houston Journal of Mathematics.

CREVELING, H. F., DEPAZ, J. F., BALADI, J. Y. & SCHOENHALS, R. J. 1975 Stability characteristics of a single-phase free convection loop. *Journal of Fluid Mechanics* **67**, 65–84.

FORNBERG, B. 1998 *A Practical Guide to Pseudospectral Methods.* Cambridge University Press.

GELFAND, I. M. & FOMIN, S. V. 1991 *Calculus of Variations.* Dover.

GLENDINNING, P. 1994 *Stability, instability and chaos: an introduction to the theory of nonlinear differential equations.* Cambridge University Press.

https://doi.org/10.1017/S0022112005006361 Published online by Cambridge University Press

Gottlieb, D. & Orszag, S. A. 1977 *Numerical Analysis of Spectral Methods: Theory and Applications.* Philadelphia: SIAM.

Greif, R. 1988 Natural circulation loops. *Heat Transfer* **110**, 1243–1257.

Greif, R., Zvirin, Y. & Mertol, A. 1979 The transient and stability behavior of a natural convection loop. *Trans. ASME* **101**, 684–688.

Hendrickson, B. & Leland, R. 1995 The Chaco user's guide: Version 2.0. *Tech. Rep.* SAND94–2692, Sandia National Labs, Albuquerque, NM.

Hughes, T. J. R., Franca, L. P. & Hulbert, G. M. 1989 A new finite element formulation for computational fluid dynamics: VIII. the Galerkin/least-squares method for advective-diffusive equations. *Comput. Meth. Appl. Mech. Engng* **73**, 173–189.

Japikse, D. 1973 Advances in thermosyphon technology. In *Advances in Heat Transfer* (ed. T. F. Irvine & Hartnett), vol. 9, pp. 1–111. Academic.

Joseph, D. D. 1976 *Stability of Fluid Motions I.* Springer.

Keener, J. P. 1995 *Principles of Applied Mathematics.* Reading, Massachusetts: Perseus Books.

Keller, J. B. 1966 Periodic oscillations in a model of thermal convection. *Journal of Fluid Mechanics* **26**, 599–606.

Landau, L. D. & Lifshitz, E. M. 1987 *Fluid Mechanics, 2nd Edn.: Course of Theoretical Physics, Vol. 6.* Butterworth-Heineman.

Lehoucq, R. & Salinger, A. 2001 Large-scale eigenvalue calculations for stability analysis of steady flows on massively parallel computers. *Intl J. Numer. Meth. Fluids* **36**, 309–327.

Lorenz, E. N. 1963 Deterministic nonperiodic flow. *J. Atmos. Sci.* **20**, 130–141.

Martin, G. & Sloley, A. 1995 Effectively design and simulate thermosyphon reboiler systems. part i. *Hydrocarbon Processing* **74**(6), 101–109.

Morioka, N. & Shimizu, T. 1978 Transition between turbulent and periodic states in the Lorenz model. *Phys. Lett.* **66A**, 447–449.

Rodríguez-Bernal, A. & Vleck, E. S. V. 1998*a* Complex oscillations in a closed thermosyphon. *Intl J. Bifurcation Chaos* **8**, 41–56.

Rodríguez-Bernal, A. & Vleck, E. S. V. 1998*b* Diffusion induced chaos in a closed loop thermosyphon. *SIAM J. Appl. Maths* **58**, 1072–1093.

Salinger, A., Burroughs, E., Pawlowski, R., Phipps, E. & Romero, L. 2005 Bifurcation tracking algorithms and software for large scale applications. *Intl J. Bifurcation Chaos* **15**, 1015–1032.

Salinger, A. G., Devine, K. D., Hennigan, G. L., Hutchinson, S. A., Moffatt, H. K. & Shadid, J. N. 1999 MPSalsa: a finite element computer program for reacting flow problems Part 2. User's guide. *Tech. Rep.* SAND96–2331, Sandia National Laboratories, Albuquerque, NM.

Salinger, A. G., Devine, K. D., Hennigan, G. L., Moffatt, H. K., Hutchinson, S. A. & Shadid, J. N. 1996 MPSalsa: a finite element computer program for reacting flow problems Part 1. User's guide. *Tech. Rep.* SAND95–2331, Sandia National Laboratories, Albuquerque, NM.

Sano, O. 1991 Cellular structure in a natural convection loop and its chaotic behaviour. i. experiment. *Fluid Dyn. Res.* **8**, 189–204.

Shadid, J. 1999 A fully-coupled Newton-Krylov solution method for parallel unstructured finite element fluid flow, heat and mass transport. *IJCFD* **12**, 199–211.

Shadid, J. N., Salinger, A. G., Schmidt, R., Smith, T. M., Hutchinson, S. A., Hennigan, G. L., Devine, K. D. & Moffat, H. 1999 MPSalsa version 1.5, a finite element computer program for reacting flow problems Part 1: Theoretical development. *Tech. Rep.* SAND98–2864, Sandia National Laboratories, Albuquerque, NM, 1999.

Shadid, J., Tuminaro, R. & Walker, H. 1997 An inexact Newton method for fully coupled solution of the Navier-Stokes equations with heat and mass transport. *J. Comput. Phys.* **137**, 155–185.

Shimizu, T. & Morioka, N. 1978 Chaos and limit cycles in the Lorenz model. *Phys. Lett.* **66A**, 182–184.

Stern, C. H., Greif, R. & Humphrey, J. 1988 An experimental study of natural convection in a toroidal loop. *J. Heat Transfer* **110**, 877–884.

Tritton, D. 1988 *Physical Fluid Dynamics.* Clarendon.

Tuminaro, R. S., Heroux, M., Hutchinson, S. A. & Shadid, J. N. 1999 Aztec user's guide: Version 2.1. *Tech. Rep.* SAND99-8801J, Sandia National Laboratories, Albuquerque, NM.

Velázquez, J. J. L. 1994 On the dynamics of a closed thermosyphon. *SIAM J. Appl. Maths* **54**, 1561–1593.

https://doi.org/10.1017/S0022112005006361 Published online by Cambridge University Press

Wang, Y., Singer, J. & Bau, H. H. 1992 Controlling chaos in a thermal convection loop. *Journal of Fluid Mechanics* **237**, 479–498.

Welander, P. 1967 On the oscillatory instability of a differentially heated fluid loop. *Journal of Fluid Mechanics* **29**, 17–30.

Willis, G. & Deardorff, J. 1970 The oscillatory motions of Rayleigh convection. **44**, 661–672.

Yuen, P. K. & Bau, H. H. 1996 Rendering a subcritical Hopf bifurcation supercritical. *Journal of Fluid Mechanics* **317**, 91–109.

https://doi.org/10.1017/S0022112005006361 Published online by Cambridge University Press